THE ROLE OF THE NUCLEUS PULPOSUS IN HUMAN INTERVERTEBRAL DISC MECHANICAL FUNCTION QUANTIFIED BY MECHANICAL LOADING AND NON-INVASIVE IMAGING

Brent L. Showalter

A DISSERTATION

in

Bioengineering

Presented to the Faculties of the University of Pennsylvania

In Partial Fulfillment of the Requirements for the Degree of Doctor of Philosophy

2015

Supervisor of Dissertation

_____
Dawn M. Elliott
Professor of Biomedical Engineering, University of Delaware

Graduate Group Chairperson

_____
Jason A. Burdick
Professor of Bioengineering

Dissertation Committee:

Beth A. Winkelstein, Professor of Bioengineering
James C. Gee, Associate Professor of Radiologic Science
Louis J. Soslowsky, Fairhill Professor of Orthopaedic Surgery
Neil R. Malhotra, Assistant Professor of Neurosurgery

ACKNOWLEDGMENTS

Dawn has played the role of advisor perfectly; in many ways, her performance has been nothing short of miraculous. She has always made time to take a very personal interest in my work. In addition, she has gone out of her way to make professional opportunities for me in an effort to both make me a better graduate student and prepare me for future employment. On top of that, she's also continued to find ways to improve my working environment, despite the fact that for several years we've worked at separate universities. On a personal level, she has been a wonderful mentor and incredibly understanding as my family has passed through unexpected difficulties. The endless stream of toys and clothes that she's given to my kids will remain household reminders of her generosity for years to come.

My thesis committee, Drs. Beth Winkelstein, Jim Gee, Lou Soslowsky, and Neil Malhotra, have had many direct and positive contributions to this thesis. As a result, this work is much better than the experiments I originally proposed. That alone marks them as a fantastic committee, but on top of that, Drs. Malhotra and Gee have at various times adopted me as part of their labs. Thank you for taking me in and teaching me to become a better scientist. Thanks also to Drs. Ed Vresilovic and Alex Wright for being friends and unofficial committee members whose questions have provided fuel for many interesting discussions.

Many thanks are due to past and present members of the Elliott Lab. Our discussions of each other's manuscript drafts epitomize the way in which our lab works together. Whether the draft is initially in good or bad condition, the discussion always lasts three hours and the manuscript leaves in much better condition. The time commitment given to thoughtfully read, edit, and discuss one another's manuscripts is given selflessly and is indicative of many other collegial kindnesses. I'm also especially grateful for the undergraduates who have worked with me over the years: Elizabeth Beattie, Ian MacLean, Dhara Amin, and Jessica Lewis. Without their work and efforts, these experiments never would have been completed.

Zeke Hernandez gets special recognition as my friend who, outside of Dawn and committee members, has had the most positive influence on my graduate studies. Zeke is a professor at Wharton whose family has gone through some of the same medical difficulties as my own. Since meeting him a year ago, his encouragement, advice, and example on balancing career and family life has been instrumental in making the final year of my studies the most enjoyable and productive of my tenure.

My family is wonderful. My parents, Mark and Marlene, are enthusiastic and fun to be around. My four sisters are angels. Most recently, my sister Holly earned her wings by completing 20 images segmentations needed for the internal strain

experiment described in Chapter 7. I love seeing my daughter Julia, 6, and son Ryan, 3, grow and explore the world. Their hugs make any day infinitely better.

This acknowledgement would be glaringly deficient if I didn't mention my wife, Jenny. In much the same way, my life would be unbearably empty without her. Her warmth, laughter, insight, intelligence, sincerity, frivolity, and a host of other attributes fill my life with meaning and daily give me something to look forward to. Our experiences in Philadelphia have welded us inseparably together and I look forward to sharing a long life with her.

ABSTRACT

THE ROLE OF THE NUCLEUS PULPOSUS IN HUMAN INTERVERTEBRAL DISC MECHANICAL FUNCTION QUANTIFIED BY MECHANICAL LOADING AND NON-INVASIVE IMAGING

Brent L. Showalter

Dawn M. Elliott

The intervertebral disc performs the mechanical roles of supporting loads, permitting motion, and dissipating energy. Disc degeneration affects a large portion of the population, reduces the joint's effectiveness, and is strongly implicated as a cause of low back pain. Degeneration is an irreversible process that manifests early within the centralized nucleus pulposus and subsequently affects other disc components. An incomplete understanding of the role of the nucleus pulposus and how alterations in nucleus function affect disc mechanics has hindered successful development of disc degeneration treatment. The objective of this dissertation was to evaluate the mechanical contributions of the nucleus pulposus to intervertebral disc function in compressive loading. In cyclic loading experiments, it was determined that removal of the nucleus pulposus via nucleotomy caused acute changes to the disc's mechanical response such as a decrease in compressive

stiffness with an accompanying increase in compressive strain. These changes correspond to hypermobility, which alters overall spinal mechanics and may impact low back pain via altered motion throughout the spinal column. In addition to these acute changes, nucleotomy also decreased the fluid-flow related effects of cyclic compressive loading. Filing the void left by nucleotomy with a hydrogel implant preserved the creep response of the discs. A procedure for creating disc strain templates, which describe average disc strain, from MR images taken before and after loading was developed to non-invasively measure internal disc strains that result from compression loading. In mildly-degenerate human discs, removal of the nucleus increased axial strain throughout the annulus fibrosus, consistent with the existing literature stating that the nucleus plays a significant role in supporting compressive loads. Removal of the nucleus also unevenly altered the distribution of circumferential and radial strains within the annulus. Nucleotomy caused substantially higher circumferential strain in the posterolateral region, which may increase the risk of annular tears. The novel tools developed in this work and the experimental results can be utilized to further understand the mechanical role of the nucleus pulposus on intervertebral disc function, how that role changes with degeneration, and to design and treatments that restore disc mechanics.

TABLE OF CONTENTS

LIST OF TABLES

LIST OF FIGURES

CHAPTER 1: Introduction

The intervertebral disc performs the mechanical roles of supporting loads, permitting motion, and dissipating energy.[87; 146] Disc degeneration affects a large portion of the population, reduces the joint's effectiveness, and is strongly implicated as a cause of low back pain.[3; 5; 59; 131; 139; 140; 148] Degeneration is an irreversible process that manifests early within the centralized nucleus pulposus and subsequently affects other disc components.[3] Current surgical treatments aim to treat the end stages of the disorder using procedures such as disc removal with subsequent fusion of the adjacent vertebrae. While these treatments reduce symptoms, they are palliative only, do not restore healthy disc function, and often ultimately fail.[9; 79; 113] The current difficulties of treating end-stage degeneration are incentive to develop treatments for earlier stages that are capable of preserving disc function and slowing the degenerative process.[17]

An incomplete understanding of the critical factors of disc degeneration has hindered successful treatment development.[6; 80; 117; 145] One degeneration mechanism is that changes within the nucleus pulposus alter how the disc supports loads, which in turn causes structural defects in other disc components.[3; 59] In an effort to examine this pathway, the objective of this dissertation was to evaluate the mechanical contributions of the nucleus pulposus to the function of the intervertebral disc in compressive loading.

Chapter 2 begins with a more thorough background on the intervertebral disc, disc degeneration, and known role of the nucleus pulposus in disc mechanics. The nucleus pulposus both supports loads directly and places the fibers of the annulus fibrosus in tension.[74; 97] Most of the existing literature evaluates disc mechanics while the disc is fully hydrated. However, because the nucleus is composed primarily of water, extended loading alters the fluid distribution in the disc, which in turn affects the disc's mechanical response.[31; 64] Chapter 3 examines the role of native nucleus pulposus and the effect of degeneration on the time-dependent mechanical response of the disc. This is done using cyclic loading and hydrated recovery to compare the response of intact discs and discs following nucleotomy. The cyclic loading is extended to examine the effect of a synthetic nucleus replacement in chapter 4.

Local tissue strain can be used to examine alterations in load distributions in an effort to explain how changes within the nucleus pulposus lead to structural defects throughout the disc.[30; 102] A technique was recently developed for non-invasively measuring 3D internal strains by acquiring MR images before and after an intervertebral disc was loaded. [157] Unfortunately, variation between samples hindered data analysis. In this work, Chapter 5 describes the development of a disc strain template, which is used to reduce individual variability in internal strain while preserving group-level trends. As part of the developmental process, a finite element model was used to validate the strain template creation technique. Chapter

6 uses strain templates to measure the nucleus pulposus affects on tissue strains in mildly degenerate discs.

Chapter 7 discusses general conclusions and how this work can be used in future studies, such as the study of disc degeneration, annular tears, and evaluation of treatments. This dissertation marks a significant increase in understanding the role of the nucleus pulposus in intervertebral disc mechanics.

CHAPTER 2: Background

2.1 Intervertebral Disc Structure and Function

The spine, comprised of alternating vertebrae and intervertebral discs (**Figure 1**), performs the mechanical functions of supporting loads, permitting motion, and dissipating energy.[87; 146] The primary disc components are the annulus fibrosus and nucleus pulposus (NP). The annulus consists of 0.11-0.52 mm thick layers of fiber-reinforced soft tissue, with fibers oriented an average of +/- 30° from the transverse plane.[81] The fibers in the outer regions of the annulus are primarily type I collagen fibers, which compose 75-90% of dry weight. As the annulus transitions from the outer to inner layers, the layers become thicker, collagen content decreases to 40-75%, and type II collagen becomes more abundant.[10; 20; 81; 131]

The centrally located NP is primarily composed of water (75-90% wet weight), proteoglycans (20-60% dry weight), and Type II collagen (25% dry weight).[10; 131] The proteoglycans create an osmotic pressure within the disc and are responsible for drawing fluid into the center of the disc.[53; 112; 130; 138] The interplay between osmotic pressure and external loads causes 20-25% of the disc's water content to be expressed and re-imbibed daily.[86; 126] In daily activities, the NP functions by both supporting loads directly and placing the collagen fibers of the annulus fibrosus in tension.[55; 98; 114] Together, the annulus and NP function as a joint capable of withstanding large forces while permitting extensive spinal flexibility.

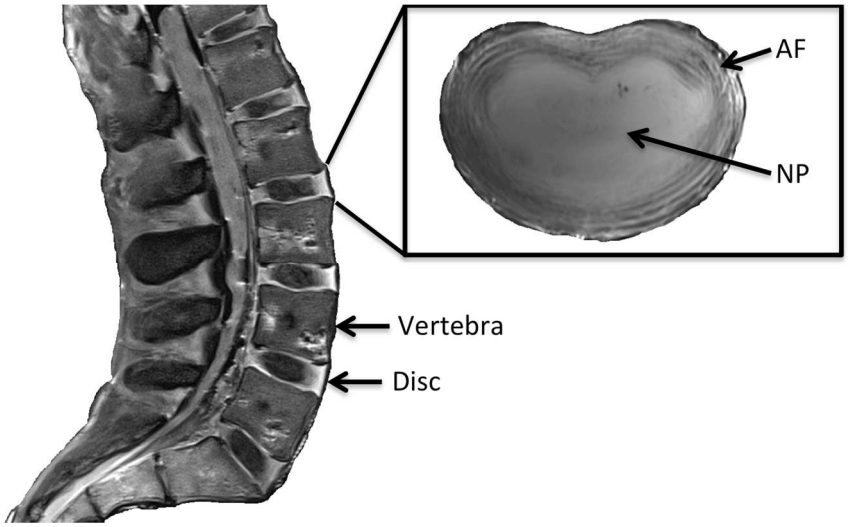

Figure 1: MR image of the lumbar spine and a cross section of an intervertebral disc with the annulus fibrosus (AF) and nucleus pulposus (NP) marked.

2.2 Disc Degeneration

The disc undergoes more dramatic alterations with age than any other muscoleskeletal soft tissue.[24] Degeneration reduces the disc's effectiveness and is strongly associated with low back pain, which causes over $100 billion in annual societal costs within the United States.[6; 9; 26; 67; 79] Disc degeneration is a multifaceted process involving structural and biochemical changes within the disc.[3; 5; 59; 131; 140; 148] These changes manifest early within the NP with decreasing proteoglycans and water content.[10] The NP becomes more fibrous as Type I collagen is replaced by Type II.[20] As a result, the NP becomes less capable of sustaining the hydrostatic pressure that places the annulus fibers in tension during loading. This leads to abnormal loading and stress concentrations within the annulus.[5] Also, the annular structure becomes more disorganized, disc height decreases, and structural defects, such as annular tears and Schmorl Nodes, develop.[4; 48; 57; 134; 143; 144] Repair and

regeneration within the disc is limited because the tissue is avascular and has low cell content.[78; 140]

Prevention and treatment of degeneration will be aided by understanding the functional role of the NP. The objective of this dissertation was to evaluate the mechanical contributions of the nucleus pulposus to the function of the intervertebral disc in compressive loading. General background on nucleotomy, cyclic loading, and internal strain measurement techniques used to accomplish this objective is found in the following sections.

2.3 Nucleotomy

The role of the NP can be determined by comparing mechanical response of intact discs with the response of discs from which the NP has been removed. NP removal is accomplished with a procedure called a nucleotomy or discectomy. Clinically, nucleotomy is performed to treat herniations by relieving pressure on the spinal cord.[43; 66; 116; 122] The procedure boasts an 80-90% success rate based on immediate symptom relief, improvement in patient metrics such as Oswerty Disability Scores, and limited reherniation rates.[44; 84; 94; 147] However, nucleotomy also alters disc mechanics by decreasing disc height, NP pressure, and stiffness while increasing range of motion and creep.[21; 25; 42; 46; 61; 63; 88; 104; 146] While these mechanical changes are clinically undesirable, they are scientifically useful because they are similar to naturally occurring degenerative changes. As a result, nucleotomy is a relevant degeneration model that can be used to evaluate mechanically based treatments such as nucleus replacements.

2.4 Cyclic Loading and Hydrated Recovery

The ability of the NP to support and transfer loads is dependent on its fluid content. As described in section 2.1, disc fluid levels fluctuate daily as a result of osmotic pressure within the NP and the external loads placed on the disc. Reduced hydration decreases disc height, increases stiffness, and increases range of motion, with properties returning to baseline after rehydration.[2; 153] These *in vivo* diurnal changes have been replicated by cyclic loading and unloaded hydrated recovery in several animal models, including porcine, ovine, and bovine.[64; 71; 135] While animal and human discs are similar, these findings may not be representative of cyclic loading in human discs due to lower water and proteoglycan content in humans, varied applied loads and loading durations between studies, and differences in cartilage endplate.[15; 37; 123; 152; 161] Disc hydration effects have also been studied using creep tests.[1; 70] However, creep induces lower fluid flow rates than cyclic loading and thus doesn't simulate the dynamic nature of disc loading.[149] In this dissertation, the time-dependent mechanical role of the nucleus pulposus was evaluated by comparing in disc's mechanical response to cyclic loading with hydrated recovery before and after nucleotomy.

2.5 Nucleus Pulposus Replacement

The current gold standard for surgical treatment of disc degeneration is fusion, in which the disc is removed and the adjacent vertebral bodies are fused.[113] While often boasting initial successful outcomes, such as reducing Oswerty Disability Index, the procedure also inherently restricts natural movement and

accelerates the degenerative process in adjacent disc levels.[56; 91] To overcome these limitations, nucleus pulposus replacements are being developed to treat early stages of degeneration while maintaining or restoring disc mechanics.[76; 105; 109; 115] Mechanical evaluation of nucleus replacements often focuses on the intrinsic mechanical properties of the implant and its immediate effects on disc mechanical response.[32; 35; 107; 114; 127] In this work, a hydrogel implant will be evaluated using moderate cyclic loading of discs followed by unloaded hydrated recovery because it is more rigorous than single cycle tests and captures elements of the time-dependent mechanical response critical for daily function.[63; 125]

2.6 Non-invasive internal disc strain

Deformation under load is a fundamental indicator of the mechanical function of a load-bearing structure. Understanding the disc's internal strain distributions for physiologically relevant loading conditions is critical for development of successful treatments designed to halt or slow the mechanical changes caused by degeneration. However, examining internal disc strains is difficult because of the layered, fiber-reinforced annulus that surrounds the pressurized NP. Previous attempts at direct measurement were either limited to surface measurements or have been invasive.[21; 88; 89; 120; 129] While these studies have provided useful information regarding the internal stress-strain distributions in the disc, the invasive methods used inherently alter the tissue structure and strain measurements. To overcome these limitations, recent research has non-invasively examined internal disc strain in using MR imaging..[29; 30; 102; 104; 157] While this is an

important improvement over invasive techniques, the MR studies have been limited to 2D slices taken in the midsaggital plane. As a result, circumferential strain cannot be measured and internal strain in damage prone regions of the disc, such as the posterolateral region, are not evaluated.

A technique capable of measuring 3D disc internal strains was recently developed.[157] In that experiment, images were taken in a 7T MR scanner using a custom designed coil capable of taking 3D images with an isotropic resolution of 0.3mm. While the strain maps calculated from these images provide unprecedented information on internal disc mechanics, individual variation between samples has hindered data analysis.

Within the field of neuroimaging, the challenge of individual variation is addressed by using data from several individuals to create templates, which are essentially averages of the imaging data.[36; 69; 108; 141; 155; 158] These templates may be single-modality, meaning that they are derived from a single imaging source, or they may be multi-modality, by utilizing information from multiple sources such as standard MRI and Diffusion Tensor Imaging.[11; 75] Because templates minimize individual variation in order to highlight key population traits, they are ideally suited for analyzing the recently acquired 3D disc images and strain maps. In this dissertation, a template creation technique was developed to better analyze this existing 3D data set to determine group-level trends in internal disc strain.

The development of templates to study tissue strain is sufficiently different from neuroimaging templates to require validation of the technique. A well-

accepted method for examining internal stress-strain profiles in biological tissues is finite element models (FEMs), and as a result, FEMs are ideal for validating the strain template technique.[98; 100; 119] Our laboratory recently created a biphasic disc FEM using the average geometry of L4-L5 disc and region specific tissue properties obtained from a wide range of experiments.[22; 23] This FEM was validated by comparing its calculated disc-level mechanical response to experimental compressive slow loading ramp, creep, and stress-relaxation tests. Because this model has undergone rigorous validation of the disc's nonlinear compression response, it is well suited for comparison to a template of MRI calculated internal strains.

After developing and validating disc internal strain templates, strain templates were then used to analyze the role of the NP in internal disc strain.

CHAPTER 3: Effect of Nucleotomy on Cyclic Loading Response of Human Discs

3.1 Introduction

Physiological cyclic compressive loading and unloaded recovery is an ideal testing modality for examining the loading contribution of the nucleus pulposus because it simulates the disc's time-dependent mechanical response. The interplay between osmotic pressure and external loads causes 20-25% of the disc's water content to be expressed and re-imbibed daily.[126] Reduced hydration decreases disc height, increases stiffness, and increases range of motion, with properties returning to baseline after rehydration.[2; 153] These diurnal changes have been replicated in several large animal models by compressive cyclic loading and unloaded recovery.[64; 71; 135] While animal and human discs are similar, these findings may not be representative of cyclic loading in human discs due to lower water and proteoglycan content in humans, varied applied loads and loading durations between studies, and differences in cartilage endplates between species.[15; 37; 123; 152; 161] Further, the majority of previous cyclic loading studies were designed to test damage mechanisms by employing high loads and number of cycles and by not including unloaded recovery.[4; 52] Disc hydration effects have also been studied using creep tests.[1; 70] However, creep induces lower fluid flow rates than cyclic loading and thus doesn't simulate the dynamic nature of disc loading.[149] This study examines the contribution of the NP to disc loading by testing human discs undergoing a

physiologically relevant testing modality, which is compressive cyclic loading with hydrated unloaded recovery.

The mechanical role of the nucleus pulposus can be evaluated by comparing the effect of cyclic loading on intact and partially nucleotomized samples. Nucleotomy, also known as discectomy, is a clinical treatment for disc herniation.[43; 66] The procedure alters disc mechanics by decreasing disc height, NP pressure, and stiffness while increasing range of motion and creep.[21; 25; 42; 46; 61; 88; 104] While the acute effects of nucleotomy have been determined, its impact on the disc's fluid-flow related mechanical response has not.

The objective of this chapter was to determine the effects of physiological cyclic loading followed by unloaded recovery on the mechanical response of human intervertebral discs. The second objective was to examine how nucleotomy alters the disc's mechanical response to cyclic loading.

3.2 Methods

3.2.1 Sample Preparation

Fifteen human lumbar spine segments with a mean donor age of 50.1 years (22-75 years) were obtained from institutionally approved sources. These spines underwent MR imaging to determine degeneration grade and T_2 relaxation times.[68; 82; 110] The L5-S1 disc was selected for testing because herniations and discectomies are most common at this level.[147] Samples had degeneration grades ranging from 1 to 5 and T_2 relaxation times ranging from 66 to 204, with higher relaxation times indicating healthier discs. T_2 relaxation time was not acquired for one sample. For

the remaining 14 samples, T_2 relaxation times correlated with Pfirrmann grades (r = -0.76) and provide a quantitative, continuous measurement of degeneration (**Figure 2**). Disc cross-sectional area was measured from MR images. After imaging, L5-S1 bone-disc-bone segments were prepared by first removing the posterior elements and extraneous soft tissue. Although *in vivo* loads are shared between the disc and facets, posterior elements were removed in order to isolate the contributions of the disc in compression.[15; 88] Following dissection, 1.25 mm Kirschner wires were placed in the L5 vertebrae and sacrum. The L5-S1 discs were wedge-shaped, with a 13±4° angle between the L5 and S1 endplates, which likely results in some applied shear loads even during simple compression experiments. For consistency in mechanical testing, loads were applied perpendicular to the L5 vertebrae. This was ensured by potting the motion segments in PMMA with the L5 endplate parallel to the potting fixtures using fluoroscopic guidance. Samples were stored in a freezer at -20°C when not in use.

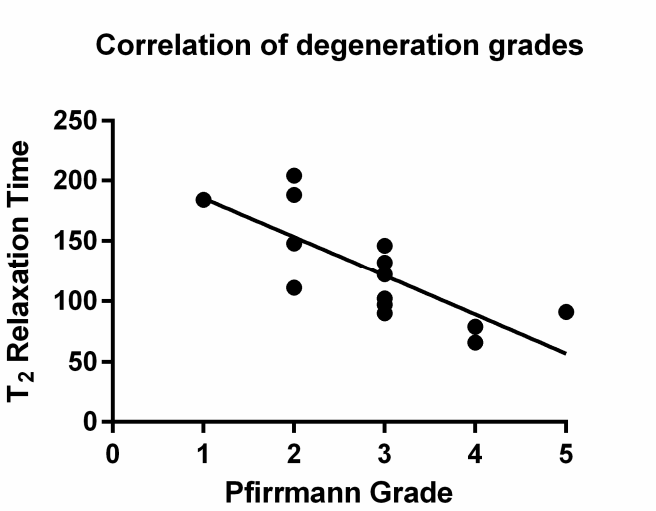

Figure 2:T2 relaxation times are strongly correlated to Pfirrmann scores (r = -0.76, p = 0.001) for the human L5-S1 discs used in this study.

3.2.2 Mechanical testing

The mechanical test consisted of six steps (**Figure 3**). 1. Overnight hydration, also called initial hydration. 2. Measure mechanical parameters (*Initial*). 3. 10,000 cycles of compressive loading. 4. Measure mechanical parameters (*Cyclic*). 5. Overnight hydration, also called unloaded recovery. 6. Measure mechanical parameters (*Recovery*). During the first step, overnight hydration, samples were submerged in a 0.15 M PBS bath containing protease inhibitors (Phenylmethylsulfonyl Fluroide, N-Ethylmalemide Bioxtra, and Benzamidine Hydrochloride from Sigma-Aldrich, St. Louis, MO) at 4°C for 16-24 hours. Second, mechanical parameters were measured by applying 60 cycles at 0.2 Hz between 0.48 MPa (734 ± 122N) in compression and 375 N in tension, which is similar to previous studies.[15] The stress of 0.48 MPa corresponds to one body weight or to

low-intensity activities such as sitting upright without support or relaxed standing.[40; 96; 153] The tensile load of 375 N was applied to all samples instead of a uniform stress to prevent sample pull out from the PMMA for discs with large cross-sectional areas while ensuring sufficient load to describe the mechanical parameters of interest. The third step was to apply 10,000 cycles of compressive loads at 2 Hz between 0.12 and 0.96 MPa (1467±244N) which are loads similar to moderate physical activities such as jogging or lifting a 10 kg weight.[96; 153] The number of cycles and cycle frequency were selected for comparison with earlier studies and because these loads are representative of moderate physical labor.[22; 64] Fourth, mechanics were measured immediately after cyclic loading in the same manner as the second step. For the fifth and six steps, discs were rehydrated overnight followed by measurement of mechanical parameters.

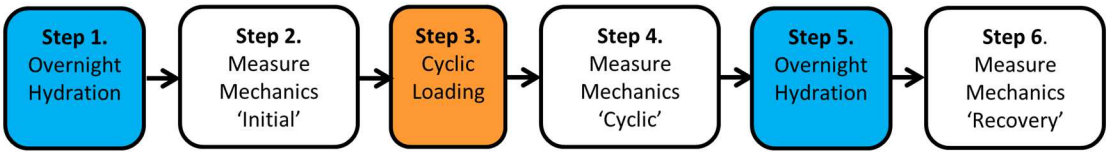

Figure 3: The mechanical testing procedure altered disc hydration. Discs are fully hydrated in a PBS bath containing protease inhibitors (Steps 1 and 5), and have reduced hydration after cyclic loading (Step 3). Mechanical parameters are measured after each change in hydration level (Steps 2, 4, and 6).

Samples were tested on an ElectroPuls E3000 test system (Instron, Norwood, MA). All tests were run using trimodal control, in which the system reaches the target peak load while running sine waves in position control. If cycle peak loads do not match the target loads, the peak positions of the sine wave are adjusted on the

next cycle. During testing, target loads were reached between the 30th and 40th cycles. While this is more preconditioning than applied in many studies, previous work showed 20 cycles were needed to sufficiently precondition the disc for measuring mechanical parameters and preliminary studies for this work showed no difference in mechanical properties measured between the 20th and 50th cycles.[19]

3.2.3 Nucleotomy

To evaluate the effect of nucleotomy, samples were tested using the 6-step method described above while intact and again following nucleotomy. Nucleotomy was performed by first hydrating the discs in PBS for eight hours. Next, a cruciate incision was created in the posterolateral annulus using a #11 scalpel blade. Afterwards, either 2 or 4 mm pituitary rongeurs were used to remove as much nuclear material as possible through the single incision, which was 1.71±0.38 g of nuclear material. This is approximately 1.7 mL and 50% of nucleus pulposus volume and is slightly less than the 2.1±0.9 g removed during a clinical discectomy.[10; 27; 39; 41] Amount of NP removed was not correlated with sample degeneration ($r = 0.19$, $p = 0.5$). Following nucleotomy, samples were frozen until further testing.

3.2.4 Data Analysis

Disc area was measured from MR images by outlining the disc in a midaxial slice using the DICOM viewer OsiriX (Pixmeo, Switzerland). Disc height was calculated from a lateral fluoroscopic image of the disc by dividing disc area by the anteroposterior width using Matlab (MathWorks, Natick, MA).[103]

The maximum position of a single loading cycle decreases over the 10,000 cycles of compressive loading (**Figure 4**). Creep was defined as the decrease in maximum cycle position from cycle 50 to 10,000 of the cyclic loading and creep strain was calculated by dividing creep by initial disc height.

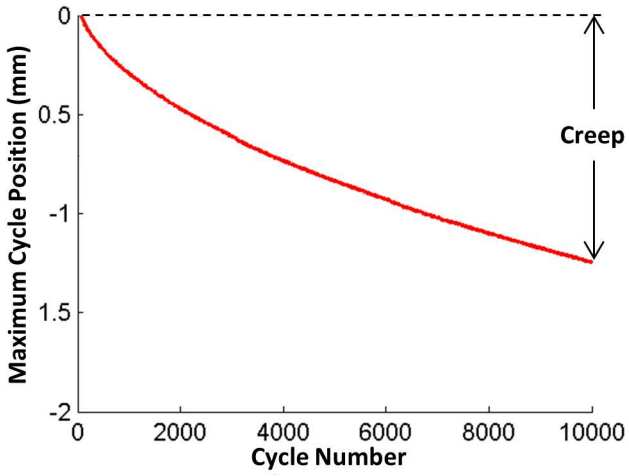

Figure 4: The maximum position of single cycle decreases throughout the 10,000 cycles of compressive loading. Creep is defined as the drop in maximum cycle displacement over 10,000 cycles, after which creep strain is calculated by dividing creep by initial disc height.

Mechanical parameters were measured on the 50th cycle of the mechanical measurement steps of the testing procedure (steps 2, 4, and 6) to ensure sufficient preconditioning and eliminate super hydration.[3; 63] Parameters were measured using a previously described custom Matlab program that performs a trilinear fit to the data (**Figure 5A**).[15] This program first determines the minimum slope location of a 5th order polynomial fit to the data (**Figure 5B**). Neutral zone stiffness was defined as the slope of the loading data at this location (**Figure 5C**). Next, the data was separated into tension and compression loading curves and compressive range

of motion was defined as the displacement between 0 MPa and 0.48 MPa of applied stress (**Figure 5D**). Compressive stiffness was defined as the slope of the line fit through the data points above 80% of the maximum compressive load (**Figure 5E**). Neutral zone length was defined as the displacement between the intersection of the neutral zone line fit with the compression and tension curves (**Figure 5F**). Compression and neutral zone apparent modulus were calculated from stiffness by multiplying by disc height and then dividing by disc area. Similarly, compression and neutral zone strain were calculated by dividing the compression range of motion or neutral zone length by disc height. Intact disc height and area were used for this normalization.

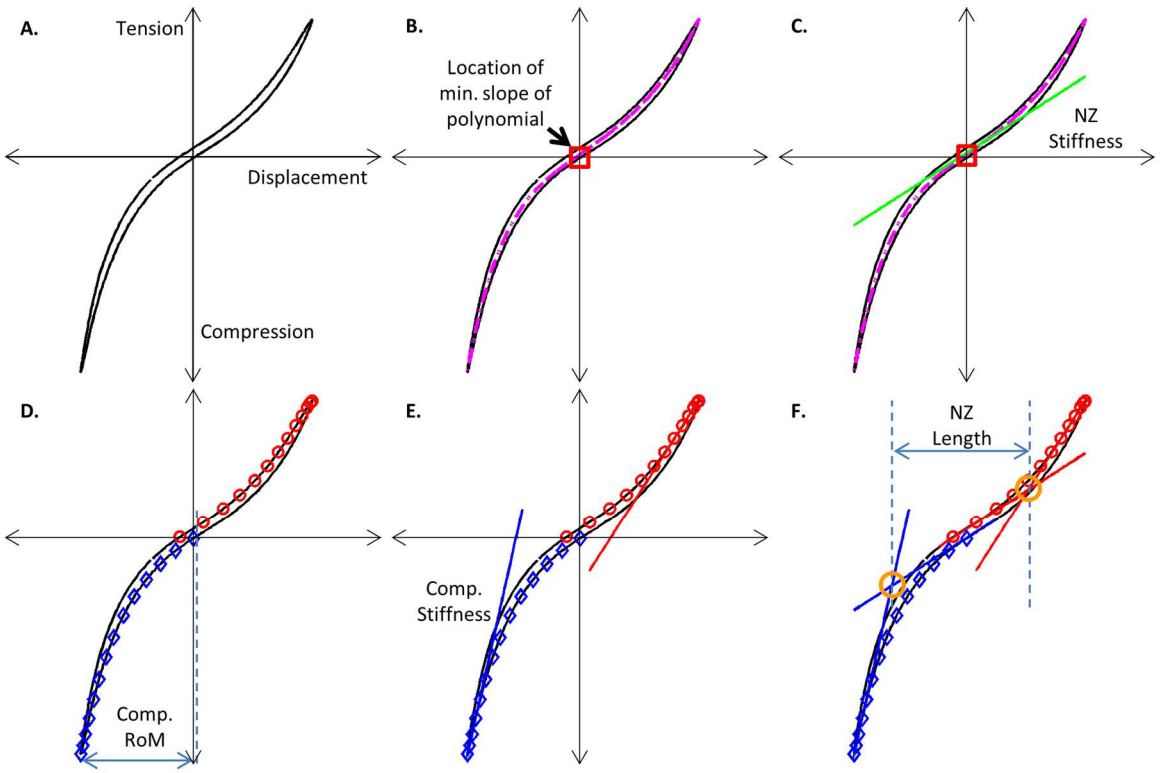

Figure 5: Mechanical parameters are found using a trilinear fit of force-displacement curve from 50th cycle of the mechanical measurement steps (steps 2, 4, and 6 of the testing procedure). A. Original data B. The minimum slope of a 5th order polynomial fit is located. C. Neutral zone is fit through data at the point of minimum slope. Neutral zone stiffness is the slope of this line. D. Tension (red circles) and compression (blue diamonds) loading curves are separated from the data. Compression range of motion is the displacement between 0 and 0.48 MPa on the compression loading curve. E. Tension and compression line fits through the maximum 80% of the respective loading curves. Compression stiffness is the slope of the compression line. F. Lines are fit in the neutral zone regions of the tension and compression loading curves. Neutral zone length is the displacement between the intersection of these lines with either the tension and compression lines. All mechanical parameters are then normalized by initial disc area and height.

3.2.5 Statistics

The effects of loading history (Initial, Cyclic, and Recovery) and treatment (Intact and Nucleotomy) on the mechanical parameters were analyzed using a 2-

Way Repeated Measures ANOVA. Significant loading histories and treatments were examined with a Tukey's or Sidak's Multiple Comparison Test, respectively. Degeneration effects on cyclic loading were examined using linear correlations between T_2 relaxation time and the percent change of parameters between loading history states. Similarly, degeneration effects on the changes caused by nucleotomy were analyzed by performing linear correlations between T_2 relaxation time and the percent change between intact and nucleotomy parameter values at respective loading history state. To include the sample with no measured T_2 relaxation time in the degeneration analysis, its T_2 relaxation time was estimated based on its Pfirrmann grade and the regression line calculated from the other 14 samples. The effects of nucleotomy on disc height and creep strain were analyzed using paired Student's t-test. Significance was set at $p < 0.05$.

3.3 Results

No visible tissue degradation was observed throughout the test. Intact disc area was 1528±254 mm^2 and disc height was 8.6±2.3 mm. Qualitatively, both nucleotomy and cyclic loading affected the load-displacement response of the disc (**Figure 6**). All mechanical data, with the exception of disc height, was normalized by disc geometry.

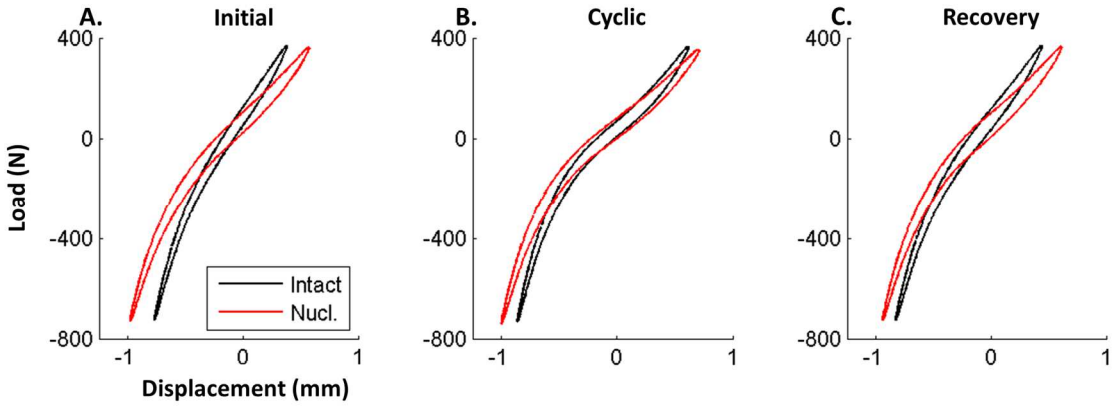

Figure 6: Force displacement curves for a single sample over the course of the experiment. Cyclic loading increased range of motion and decreased neutral zone modulus, which recovered following hydration. Nucleotomy increased range of motion while decreasing stiffness and the amount of change in mechanical parameters caused by cyclic loading.

3.3.1 Effects of Cyclic Loading Followed by Hydrated Recovery

For intact samples, 10,000 cycles of compressive loading increased compressive modulus by 3% and increased compressive strain by 33% (**Figure 7A&B**). Neutral zone properties were also affected by compressive cyclic loading, which decreased neutral zone modulus by 52% and increased neutral zone strain by 31% (**Figure 7C&D**). Unloaded hydrated recovery caused neutral zone modulus and neutral zone strain to return to initial values (**Figure 7C&D**). However, unexpectedly, compressive modulus decreased 9% from initial and compressive strain remained elevated by 16% after unloaded recovery compared to initial values (**Figure 7A&B**).

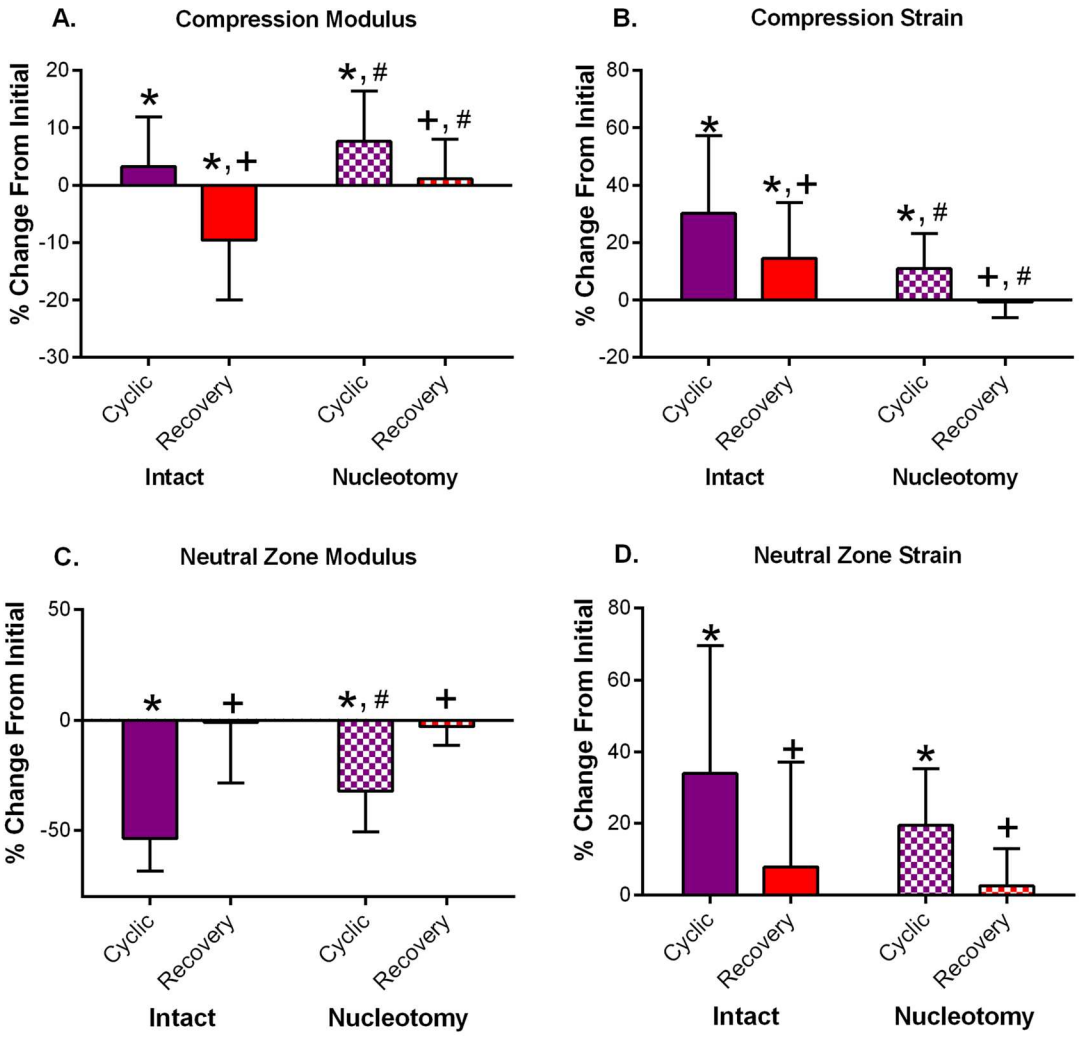

Figure 7: Disc mechanical properties are altered by cyclic loading (cyclic) and generally recover after unloaded hydration (recovery). These changes mimic naturally occurring diurnal changes. Nucleotomy reduced the hydration effects on mechanical properties. In particular, nucleotomy reduced the percent change between the Initial and Cyclic hydration states for compressive strain (B), neutral zone modulus (C), and neutral zone strain (D). *$p < 0.05$ vs. initial, $^{+}p<0.05$ vs. cyclic, # $p<0.05$ vs. intact.

Degeneration did not significantly affect cyclic loading in intact samples ($p > 0.05$). However, following nucleotomy, degeneration influenced cyclic loading effects in compressive strain, neutral zone modulus, and neutral zone stiffness (**Figure 8**). Specifically, samples with lower T_2 relaxation times (more degenerate samples) had greater increases in compressive strain between the initial and cyclic time points ($r = -0.53$, $p = 0.04$) and similarly had larger decreases in compressive strain between the cyclic and recovery time points ($r = 0.54$, $p = 0.04$) (**Figure 8B**). More degenerate samples also experienced greater changes in neutral zone mechanics. Low T_2 relaxation times corresponded to greater decreases in percent change of neutral zone modulus ($r = 0.72$, $p = 0.002$) and increases in percent change of neutral zone strain ($r = -0.70$, $p = 0.004$) between the initial and cyclic time points (**Figure 8C&D**). These greater changes between the initial and cyclic time points were matched by similar greater magnitudes of restoration towards initial values between the cyclic and recovery time points.

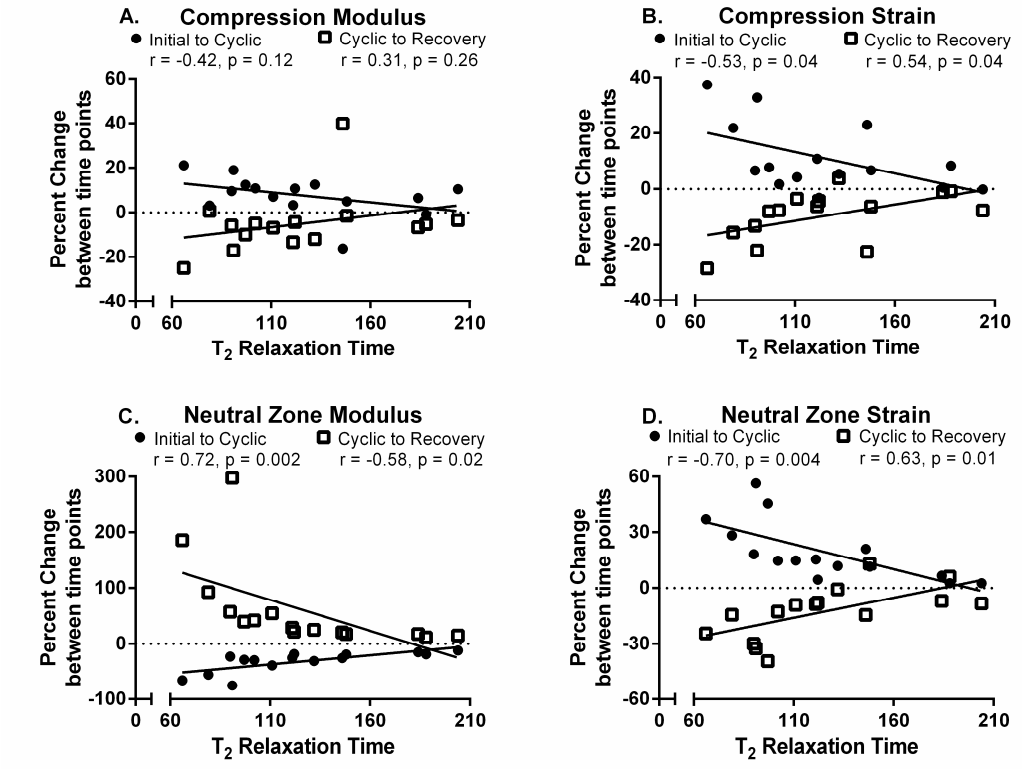

Figure 8: Impact of degeneration on the percent change of mechanical parameters caused by cyclic loading in nucleotomy samples. More degenerate samples (Lower T_2 Relaxation Time) experienced non-significant increases in compression modulus (A) and significant increases in both compression and neutral zone strain (B&D) as a result of 10,000 cycles of compressive loading, and proportional decreases following unloaded recovery. More degenerate samples also experienced greater decreases in neutral zone modulus (C) following cyclic compressive loading and corresponding greater recoveries following unloaded recovery.

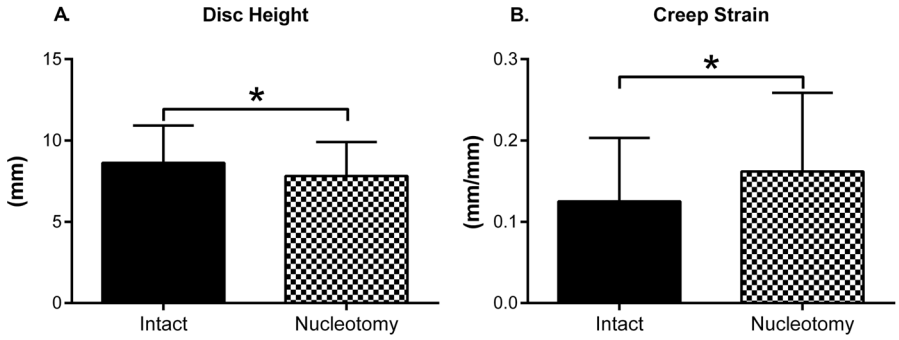

Figure 9: Nucleotomy decreased disc height and increased creep strain.

3.3.2 Effects of Nucleotomy

Nucleotomy reduced disc height by 9% and caused a 29% increase in creep strain (**Figure 9**). Compression apparent modulus decreased 19, 15, and 9% at the initial, cyclic, and recovery time points, respectively (**Figure 10A**) and was accompanied by corresponding increases in compressive strain of 38, 19, and 19% (**Figure 10B**). Nucleotomy decreased neutral zone modulus by 16 and 13% (**Figure 10C**) at the initial and recovery time points, but increased it by 31% at the cyclic loading condition. The procedure also caused increases in neutral zone strain of 18, 11, and 15% at the three loading conditions (**Figure 10D**). These findings indicate that nucleotomy induces hypermobility regardless of the disc's hydration state. Sample degeneration did not affect the changes caused by nucleotomy ($p > 0.28$).

Following nucleotomy, cyclic loading affected the compressive and neutral zone mechanical properties in the same direction as the intact samples (e.g. compressive modulus increased for both intact and nucleotomy samples), but change in magnitudes were different. Specifically, after nucleotomy, cyclic loading increased compressive modulus by 7% and compressive strain by 15%. Neutral zone modulus decreased by 25% and neutral zone strain increased by 23%. For nucleotomy samples, all mechanical parameters returned to initial values following a period of unloaded hydrated recovery (**Figure 7A-D**).

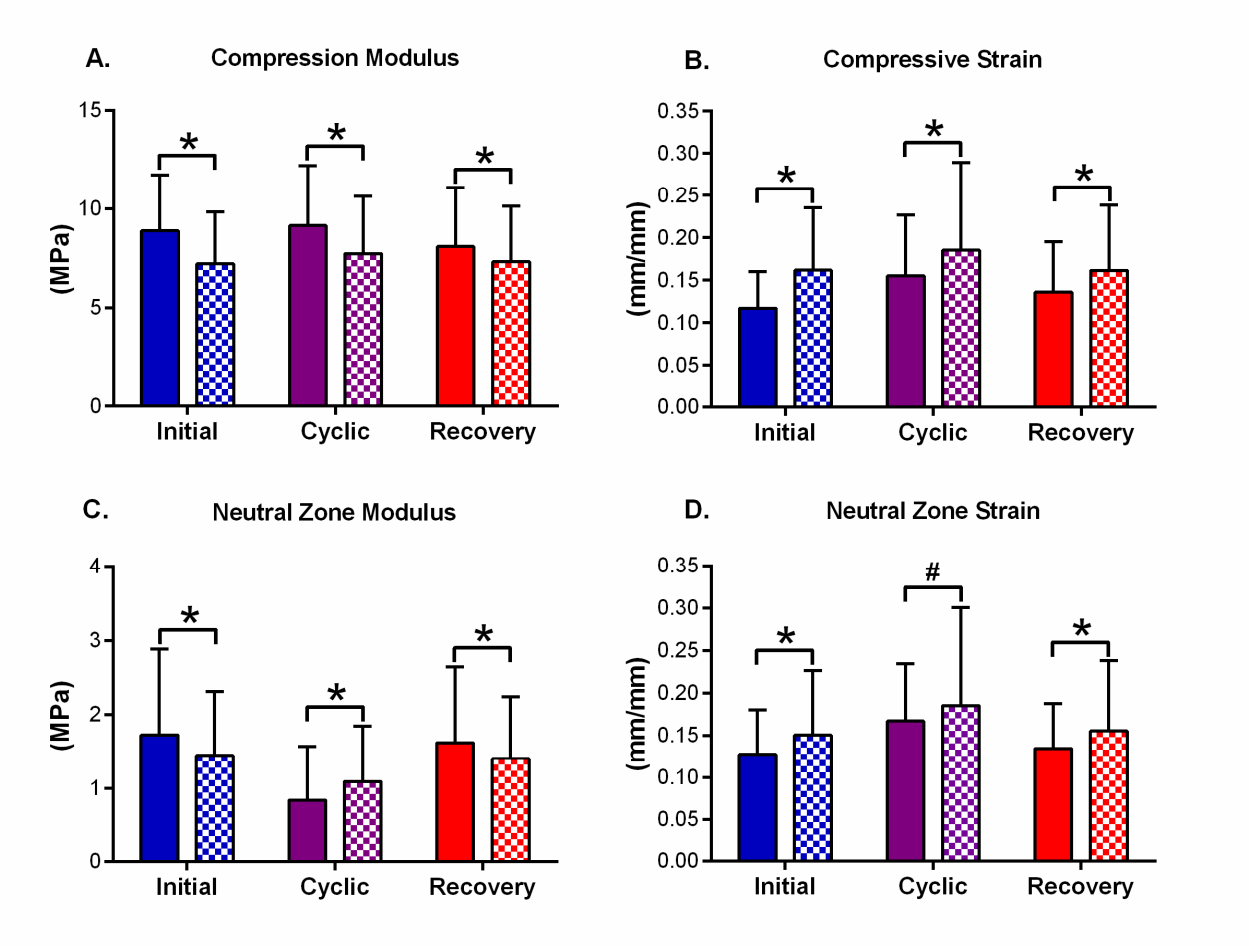

Figure 10: Nucleotomy decreased compression modulus (A), increased compressive strain (B), decreased neutral zone modulus at the initial and recovery hydration states and increased neutral zone modulus at the cyclic hydration state (C), and increased neutral zone strain (D). These findings indicate that nucleotomy induces hypermobility regardless of the disc's hydration state. Solid = Intact, Checkered = Nucleotomy. *$p < 0.05$, #$p < 0.1$

3.3.3 Interaction of Nucleotomy and Cyclic Loading

There was a significant interaction between nucleotomy and loading history for compression modulus, compression strain, and neutral zone modulus. Nucleotomy increased the magnitude of the percent increase in compression modulus caused by cyclic loading (**Figure 3**, step 3) from 3% for intact samples to 7% following nucleotomy (**Figure 7A**). However, the procedure also reduced the

percent change caused by cyclic loading in compression strain from 33% for intact samples to 15% (**Figure 7B**) and percent change in neutral zone modulus decreased from 52% for intact samples to 25% following nucleotomy (**Figure 7C**). Nucleotomy also affected the trends caused by unloaded recovery (**Figure 3**, step 5). Compressive modulus decreased by 12% following unloaded recovery for intact samples, but was only 5% lower for nucleotomy samples. For intact samples, compressive strain decreased by 12% following unloaded recovery, which increased to 13% for nucleotomy samples. Unloaded recovery increased neutral zone modulus by 94% for intact samples, but only 29% for nucleotomy samples.

3.4 Discussion

The first study objective was to determine the effects of physiological cyclic loading followed by unloaded recovery on the mechanical response of human intervertebral discs. We determined that human discs were less affected by cyclic loading than animal models in previous studies and that cyclic loading affected neutral zone properties more than compressive properties. The second objective was to examine how nucleotomy alters the disc's mechanical response to cyclic loading. We found that partial removal of the nucleus pulposus decreases intervertebral disc modulus while increasing strain (range of motion), which corresponds to hypermobility. Nucleotomy also mitigated cyclic loading effects on mechanical properties, indicating altered fluid flow. This altered fluid flow may in turn affect cellular mechanotransduction and transport of disc nutrients and waste.

In human discs, cyclic loading and hydrated recovery affected both compressive and neutral zone properties. For example, cyclic loading increased compressive modulus by 3% while recovery decreased it by 12% (**Figure 7A**). This is lower than the 15-33% changes seen in bovine and ovine tests.[64; 71] However, the lower magnitudes were expected because the mechanical changes are due to redistribution of fluid within the disc and human discs have a lower fluid content than the animal discs.[2; 64]

Cyclic loading caused greater changes in neutral zone properties than compressive properties (**Figure 7**). Cyclic loading effects on neutral zone properties have not previously been reported; however, the role of the nucleus is more pronounced in the neutral zone than at higher loads.[25] Given that cyclic loading causes fluid to be either redistributed within or extruded from the disc and that the NP has higher water content than the annulus,[10; 64] higher fluid flow from the nucleus may explain why neutral zone properties were more affected by cyclic loading than compressive properties.

An intriguing result of the study is the limited role degeneration plays in affecting the disc's mechanical response to cyclic loading and hydrated recovery. Degeneration was correlated with cyclic loading effects after nucleotomy (**Figure 8**), with more degenerate samples experiencing greater increases in both compressive and neutral zone strain following cyclic loading. However, degeneration was not correlated with the acute changes of nucleotomy or effect of cyclic loading in intact discs. The more disorganized annular structure of the degenerate samples likely

permits greater redistribution of fluid than is possible for intact samples, which was magnified by the nucleotomy incision.[48; 90] This finding has clinical relevance, indicating that nucleotomy causes more hypermobility in extended physiological loading for degenerate discs than non-degenerate discs.

The acute effects of nucleotomy were a loss of disc height, decrease in both compressive and neutral zone modulus, and increase in compressive and neutral zone range of motion (**Figure 9** & **Figure 10**). Decreased disc height and increased range of motion caused by nucleotomy indicate that in order to compensate for the disc's altered mechanical loading following nucleus depressurization (via age-related proteoglycan loss, herniation, or discectomy) the remaining annulus and surrounding spinal elements must resist more motion. This could induce back pain by placing additional stresses on these innervated structures and advancing the degenerative cascade. In addition, spinal motion of the treated and adjacent levels may be altered if facet joints induce flexion moments within the disc. Also, the mechanical changes of nucleotomy are similar to the mechanical changes of natural degeneration. Thus, nucleotomy is a potential platform for evaluating mechanically based spinal treatments, such nucleus pulposus replacement.[105; 118; 154]

Our measured acute effects of nucleotomy are comparable to literature values. Specifically, our measured disc height loss of 0.8 mm for 1.71 g of NP removed is comparable to a reported height loss of 0.5 mm for 1.75 g removed.[151] Our observation that nucleotomy initially causes a 0.35 mm increase in compressive range of motion is lower than literature values of 0.6-0.8 mm.[42; 104] However, these

studies also applied higher compressive loads, which may account for some of this difference. In addition, the unique geometry of the L5-S1 disc relative to the other lumbar levels used in the existing literature may further explain these differences. Our observed 20% decrease in compressive stiffness fits within the literature range of 3-50% decrease for trans-annular nucleotomy studies.[25; 83] However, trans-endplate nucleotomy did not affect compressive stiffness,[63] which suggests that the decreased compressive stiffness caused by nucleotomy may be more the result of the annular injury than the removal of the nucleus. This is corroborated by existing literature that shows the annulus plays a significant role in supporting compressive loads.[58; 146]

It's interesting that the NZ modulus at the cyclic time point is higher for the nucleotomy sample than for the intact samples (**Figure 10C**). The higher modulus after nucleotomy may be attributed to fluid flow through the annular nucleotomy incision. In intact samples, the annulus serves as a barrier for fluid flow to and from the nucleus. The incision may increase permeability or create a fluid flow channel in the injury region.[90] As a result, following nucleotomy, PBS from the bath may more freely enter and exit the disc. Thus, the neutral zone modulus of nucleotomy samples at the cyclic time point may be higher than intact samples because there is more PBS within the nuclear region.

In addition to the acute effects of nucleotomy, we also found that nucleotomy reduced cyclic loading effects. This is clearly seen in the reduction of percent change between cyclic and recovery values for compressive modulus (12 to 5%) and

neutral zone modulus (94 to 29%) (**Figure 7A&C**). Reduced effects of cyclic loading indicate altered fluid flow, which has two significant ramifications. First, it alters the stresses and strains experienced by the disc's cells, potentially altering cellular mechanotransduction and subsequent protein synthesis.[121] This in turn, may alter the discs biochemical composition and mechanical function.[13] The second potential effect of altered fluid flow is modified nutrient delivery and waste removal. The intervertebral disc is a largely avascular tissue and, as a result, its cells are dependent on nutrient diffusion.[93; 139] Thus, any alterations to the delivery mechanism have the potential to create wide-reaching effects.

The failure of compressive modulus and compressive strain to return to initial values for the intact samples (**Figure 7A&B**) indicates a study limitation in that cyclic loading may have caused some non-recoverable damage to the annulus fibrosus. However, following annular nucleotomy, the compressive properties at the initial and recovery hydration states are identical. This suggests the damage caused to the intact samples is due to resisting fluid flow through the annulus, because following nucleotomy fluid had a less obstructed pathway. This potential annular damage was unexpected because it was not seen in previous ovine studies with similar loads or in the preliminary studies for this work.[64; 80] However, most of the human tissue used was moderately degenerated, in contrast with the non-degenerate samples used in animal studies. This initial degeneration may have caused the samples to be more susceptible to injury. In contrast to compressive

properties, cyclic loading effects in neutral zone properties were completely recoverable following hydration.

This study has demonstrated that cyclic loading increases compressive modulus, compressive strain, and neutral zone strain while decreasing neutral zone modulus. These changes are the result of altered hydration levels caused by the cyclic loading protocol and are similar to naturally occurring diurnal changes. Nucleotomy reduced disc height and modulus while increasing range of motion. In addition to these acute changes, nucleotomy also reduced the difference between mechanical properties before and after cyclic loading. The observed changes in mechanical behavior induced by nucleotomy are similar to naturally occurring degenerative changes. Results of this study provide an ideal protocol and control data for evaluating the effectiveness of a mechanically-based disc degeneration treatment, such as a nucleus replacement.

CHAPTER 4: Effect of Hydrogel Implant on Cyclic Loading of Human Discs

4.1 Introduction

Despite the prevalence of disc degeneration and its contributions to low back problems, many current treatments are palliative only and ultimately fail.[9; 79; 113] The current gold standard for surgical treatment is fusion, in which the disc is removed and the adjacent vertebral bodies are fused.[113] While often boasting initial successful outcomes, such as reducing Oswerty Disability Index, the procedure also inherently restricts natural movement and accelerates the degenerative process in adjacent disc levels.[56; 91] More recently, total disc replacements have sought to treat low back problems while retaining motion.[16] However, current replacements do not match native non-degenerative mechanical function, are subject to wear and failure, and resection is associated with risk of significant complications.[38; 73] The pervasiveness of disc degeneration coupled with the failures and complications associated with the current treatments indicate a pressing need for improved treatments that permit the disc to perform its primarily mechanical functions.

Nucleus pulposus replacements designed to treat early stages of degeneration while maintaining or restoring disc mechanics are under development.[76; 105; 109; 115] In this chapter, we evaluated an in situ gelable, triple-interpenetrating-network hydrogel nucleus replacement. The gel is composed of n-carboxyethyl chitosan, oxidized dextran, and teleostean and is well suited as a

nucleus replacement in part because after mixing it solidifies rapidly at body temperature and demonstrates increased resistance to biodegradation relative to single-network hydrogels.[160] It has also recently been demonstrated that the gel maintains cell viability, promotes proliferation, and has mechanical properties similar to native human nucleus pulposus.[128] A similar hydrogel restored compressive range of motion in single-cycle tests of injured ovine discs.[80] However, it remains unknown if this hydrogel implant will be contained in more extensive mechanical tests and if it will restore mechanics in injured human discs.

Mechanical evaluation of nucleus replacements often focuses on the intrinsic mechanical properties of the gel and its immediate effects on disc mechanical response.[32; 35; 107; 114; 127] More extensive mechanical testing is completed with the aim of testing failure properties.[17; 54] While not commonly used, moderate cyclic loading of discs followed by unloaded hydrated recovery is a valuable testing modality because it is more rigorous than single cycle tests and captures elements of the time-dependent mechanical response critical for daily function.[63; 125] Within the disc, interplay between osmotic pressure and external loads causes 20–25% of the disc's water content to be expressed and re-imbibed daily (Sivan et al., 2006). Reduced hydration decreases disc height, increases stiffness, and increases range of motion, with properties returning to baseline after rehydration (Adams et al., 1990; Wilke et al., 1999). Cyclic loading followed by hydrated recovery in human discs mimics this naturally occurring diurnal response.[125] In a previous study that used cyclic loading to evaluate a hydrogel implant in injured porcine discs, the implant

demonstrated recovery of angular stiffness and disc height.[14] However, that study did not evaluate the effects of hydrated, unloaded recovery and thus could not evaluate the time-dependent mechanical response. Also, human discs have greater degeneration and lower water content than animal discs, which may affect an implant's ability to improve disc function. The objective of this chapter was to determine if the hydrogel implant will be contained and if it will restore mechanics in human discs undergoing physiologic cyclic compressive loading with unloaded hydrated recovery.

4.2 Methods

Fourteen human lumbar spine segments were tested using physiologic cyclic compressive loading while intact, following nucleotomy, and again following treatment of injecting either PBS (sham, n=7) or hydrogel (implant, n=7).

4.2.1 Sample Preparation and Mechanical Testing

Fourteen human lumbar spine segments with a mean donor age of 49.5 years (22-75 years) were obtained from institutionally approved sources. These are the same samples that were used in for the nucleotomy cyclic loading experiment described in the previous chapter.

4.2.3 Treatment

Samples were separated into sham and implant groups based on blocked randomization of intact initial compressive strain. Prior to injection, discs were hydrated in PBS at 37°C. Both sham and implant groups received an injection to fill

the void created by nucleotomy (0.5±0.02 mL). The nucleus pulposus remaining in the disc following during nucleotomy expanded during rehydration and as a result, less material was injected than was removed. Sham samples (n=7) received an injection of the PBS, while the implant group (n=7) received an injection of the hydrogel implant. The hydrogel implant was created by mixing aqueous solutions of 20% teleostean, 3% N-carboxyethyl chitosan and 7.5% oxidized dextran were at a ratio of 1:1:2.[160] Toluidine blue was mixed in the aqueous solution of teleostean before mixing the hydrogel components to permit visualization of the implant. After injection, both sham and implant groups were placed in a PBS bath held at 37°C to allow the implant to cure. It is likely that the PBS from the sham injection and the bath were interchanged during this period. However, the implant mixture cured sufficiently in the few minutes prior to placement in the PBS bath that the gel was not observed to be dispersed in the bath during the curing period. Afterwards, samples were mechanically tested as described in section 3.2.2.

4.2.4 Data Analysis and Statistics

Disc height, creep during cyclic loading, compression modulus, and compression strain were defined and calculated as described in section 3.2.4.

The effects of treatment (Sham and Implant) and loading history (Initial, Cyclic, and Recovery) on the mechanical parameters (compression modulus and compression strain) were analyzed using a 2-Way ANOVA with repeated measures for loading history. Significant treatments and loading histories were analyzed with a Sidak's Multiple Comparison Test.

Degeneration effects on cyclic loading for implant and sham groups were examined using linear correlations between T_2 relaxation time of the intact samples and the percent change of parameters between the initial and cyclic time points of the treated samples. Similarly, degeneration effects on the changes caused by sham or implant treatment were analyzed by performing linear correlations between intact T_2 relaxation time and the percent change between nucleotomy and treatment parameter values at their respective loading history state (initial, cyclic, or recovery). To include the sample with no measured T_2 relaxation time in the degeneration analysis, its T_2 relaxation time was estimated based on its Pfirrmann grade and the regression line calculated from the other 13 samples.

The effect of treatment on creep strain was analyzed using a Student's t-test. Because data was taken at multiple time points for each sample, all statistical tests except for the direct comparison between sham and implant samples used repeated measured or paired statistics; that is, the statistical tests evaluated if the mean change per sample between time points was non-zero. Significance for all tests was set at $p < 0.05$.

4.3 Results

No visible tissue degradation was observed at the end of mechanical testing and no nucleus pulposus material was ejected from the sham discs. More importantly, the hydrogel implant was not ejected from the disc during testing and was undamaged when discs were bisected following all mechanical tests (**Figure 11**). As seen in the figure, implant material interdigitated with the surrounding disc

tissue. However, no physical bonds were formed between the nucleus pulposus and the implant, and minimal force could separate the gel and disc tissue. Intact disc area was 1543±233 mm^2 and disc height was 8.6±2.4 mm. Samples were separated by blocked randomization based on the compression strain of the intact disc at the initial time point. Intact initial compression strain for the sham group was 0.12±0.05 and for the implant group was 0.11±0.05, which was not statistically different (p = 0.74). All mechanical data presented is normalized by disc geometry as described in the methods section.

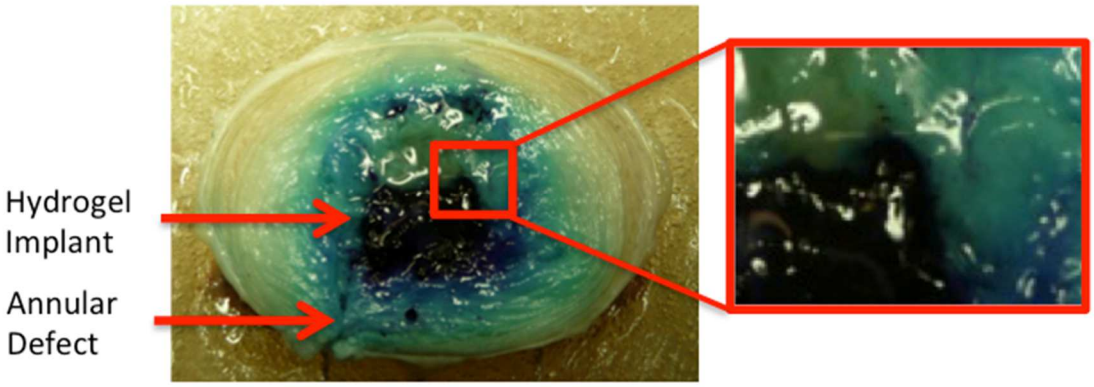

Figure 11: Bisected human L5-S1 disc after complete mechanical test, including 10,000 cycles of compressive loading. The hydrogel implant stayed intact within the disc, although some of the toluidine blue used to dye the gel leached into the surrounding disc tissue. The enlarged region shows that the implant (dark blue in lower left corner of inset) filled in the irregular contours of the remaining nucleus pulposus (light blue surrounding tissue).

4.3.1 Effect of Cyclic Loading Followed by Hydrated Recovery

Cyclic loading increased the compression modulus by 8.7±2.8% from 6.7±2.7 MPa for the sham group and by 5.5±4.1% from 7.8±2.8 MPa for the implant group (**Figure 12A**). Similarly, cyclic loading increased compressive strain by 14.4±13.4% from 0.17±0.08 for the sham group and by 13.7±9.7% from 0.15±0.09 for the

implant group (**Figure 12B**). The differences in initial values and percent increases between the sham and implant samples were not significant. Changes in compression modulus completely recovered following a period of unloaded hydrated recovery (**Figure 12A**). Compression strain partially recovered, with compression strain remaining 7.3±7.9% higher than initial for sham samples and 7.8±7.5% higher for implant (**Figure 12B**). These trends were similar to those seen for samples while they were intact and following nucleotomy.[125]

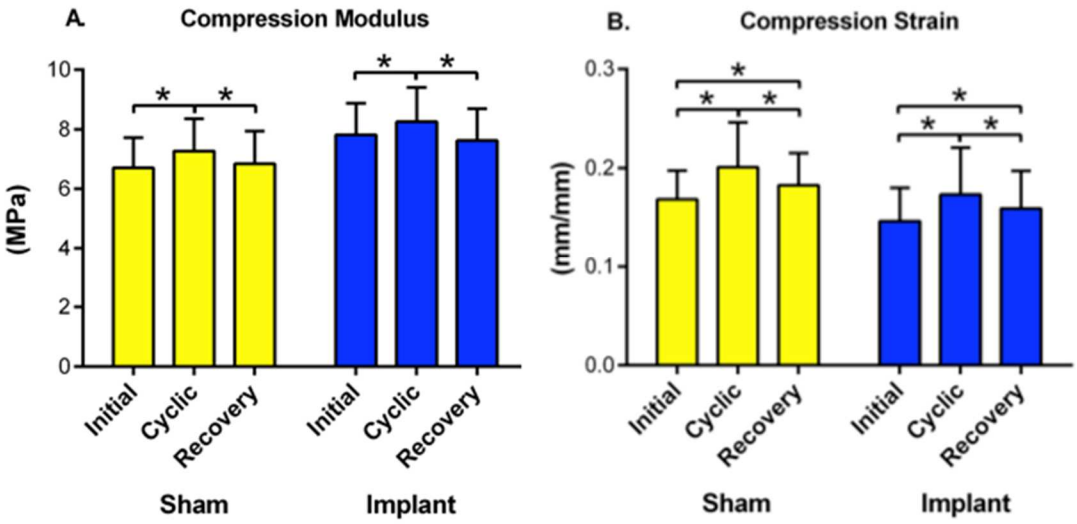

Figure 12: Cyclic loading caused an increase in compression modulus (A) and compression strain (B) for both sham and implant samples. These increases were recovered following a period of overnight hydration, indicating that the changes are due to changes in hydration distribution within the intervertebral disc. Recoverable increases in compression modulus and strain are consistent with trends in intact and nucleotomy samples. Data presented as mean + standard error. * indicates $p < 0.05$

4.3.2 Effect of Sham and Implant Treatment

Nucleotomy previously caused a 43% increase in creep strain from the intact value of 0.12±0.08 mm/mm (**Figure 13A**).[125] For sham samples, creep strain further increased by 15% from nucleotomy, while for implant samples creep strain

decreased by 3% (**Figure 13B**). The difference in creep strain between implant and sham groups was statistically significant. Nucleotomy decreased compression modulus 19% from initial intact value of 8.9±2.8 MPa and increased compression strain 38% from 0.12±0.04 mm/mm.[125] Compression modulus was not affected by either sham or implant treatment ($p > 0.2$) (**Figure 14A**). For sham samples, compression strain was 4.6±7.6% and 7.3±7.6% higher than nucleotomy values at the cyclic and recovery time points (**Figure 14B**). For implant samples, compression strain was 4.3±8.9% and 5.0±8.9% higher than nucleotomy values at the cyclic and recovery time points (**Figure 14B**). The difference in compressive strain between sham and implant samples was not significant ($p > 0.9$).

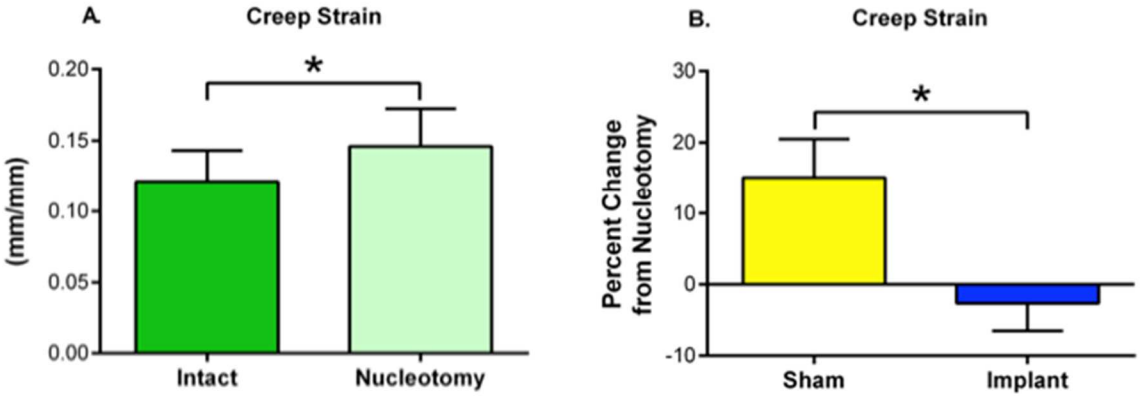

Figure 13: Nucleotomy increased creep strain (A). Following treatment, strain continued to increase for sham samples, but decreased for implant samples (B). Data presented as mean + standard error. * indicates $p < 0.05$

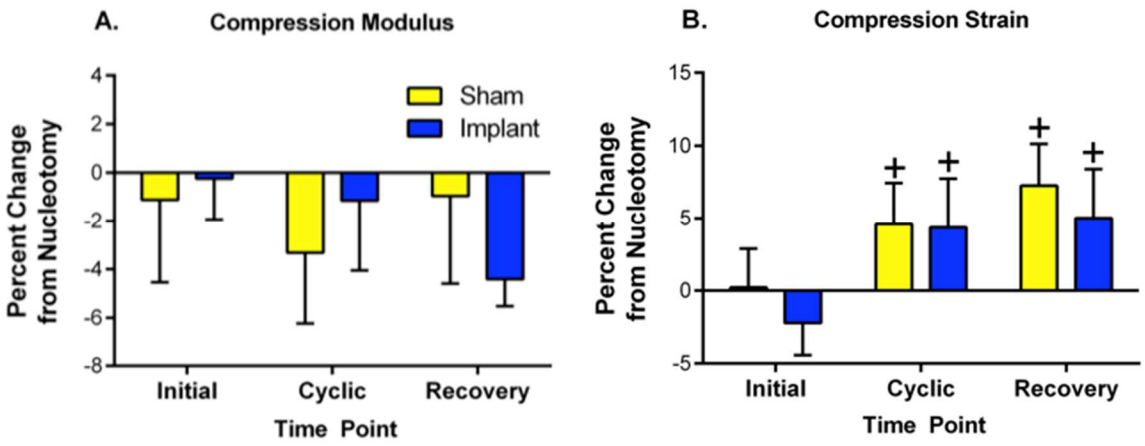

Figure 14: Percent change from nucleotomy values for sham and implant samples. Treatment caused no change in compression modulus (A). Compression strain continued to increase for both sham and implant samples at the cyclic and recovery time points (B). Data presented as mean + standard error. **+** indicates $p < 0.05$ vs. nucleotomy values

4.3.3 Effect of Degeneration

For implant samples, intact T_2 relaxation time was correlated with the amount of change in compression modulus caused by cyclic loading (**Figure 15**). There was a larger effect of the implant in more degenerated discs (e.g., those with a lower T_2 relaxation time), with a slope of -0.076 % change/ms and an intercept of 15.7%. This correlation was not significant for the intact and nucleotomy controls of the implant group ($p > 0.4$, **Figure 15**). There were no other significant correlations between T_2 relaxation time and mechanical parameters for the sham or groups ($p > 0.25$).

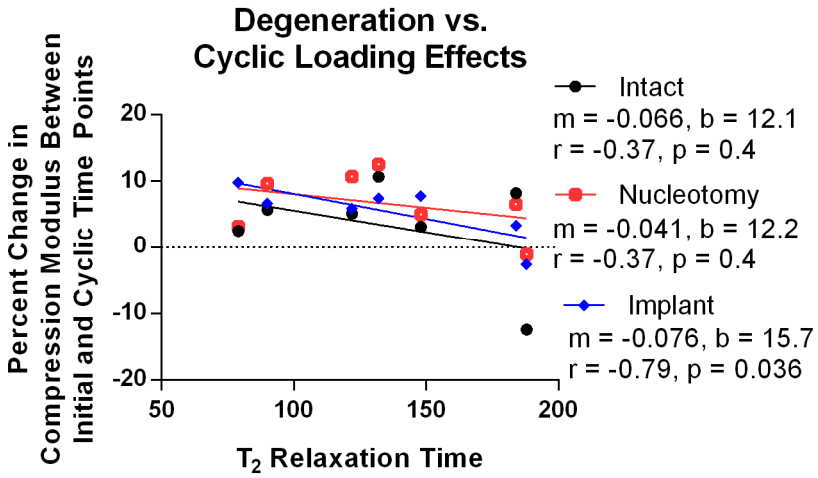

Figure 15: Percent change in compression modulus between the initial and cyclic time point for the samples in the implant group. This correlation was not significant for the samples while they were intact or following nucleotomy, but was significant following injection of the hydrogel. The slope (m) and y-intercepts (b) of the regression are show in the legend.

4.4 Discussion

The hydrogel implant presented in this work successfully remained intact and contained in human discs under physiologic cyclic compressive loads and had a positive impact on the mechanical response of the disc. Implant expulsion has been a significant problem with nucleus pulposus replacements for both human and animal studies, with expulsion rates as high as 33%.[7; 8] Some research groups have addressed this problem by developing annular repair techniques such as sutures or cyanoacrylate glue, but the long-term efficacy of such repairs has not been established.[23; 54] In this study, the hydrogel remained intact throughout the 10,000 cycles of compressive physiologic loading without repairing the large cruciate incision created during the nucleotomy procedure, which is due in part to the interdigitation of the gel with the disc (**Figure 11**). This successful result merits

further implant retention testing in more rigorous loading modalities such as bending and torsion.

The implant successfully preserved the disc's creep response, while creep strain for the sham group continued to increase the strain for the implant group remained constant (**Figure 13**). Increased creep strain indicates lower disc height for a given applied load, which in turn alters spinal motion and potentially affects low back pain.[92] The increased strain for the sham samples indicates that the mechanical test was damaging the tissue. The damage is probably due in part to the depressurization of the nucleus pulposus, which forces the annulus to carry more of the load. This finding is consistent with previous nucleotomy experiments.[80] The creep response for implant samples did not return to intact values. However, this was anticipated given that the implant did not restore the disc pressure lost in the injury procedure. The implant's ability to preserve the creep response is a positive outcome for this mechanically based treatment.

The significant correlation between degeneration and the effect of cyclic loading on the implant samples highlight the decrease in annular function with degeneration. Although the regression lines for the intact and nucleotomy tests of the same samples are similar to that of the implant treatment, the variability inherent in biological samples prevented the trends from being statistically significant ($p > 0.4$). When that biological tissue was replaced with a consistent, synthetic material, the variability seemed to decrease and correlations became significant. More degenerate discs (those with lower T_2 relaxation times),

experienced greater changes in modulus as a result of cyclic loading (**Figure 15**). As changes in cyclic loading are largely due to redistribution or expulsion of fluid within the disc,[125] greater changes in cyclic loading properties suggests that the annulus fibrosus of the degenerate samples is more permeable and less structurally coherent than those non-degenerate discs. The correlation also demonstrates that the hydrogel implant does not compensate for existing degenerative changes in the annulus. This is an expected result, and indicates that a nucleus replacement would be most beneficial for discs that had undergone degenerative changes in the nucleus pulposus, but prior to the more severe changes that subsequently occur in the annulus.

The implant did not alter the stiffening effects, and subsequent recovery, caused by cyclic loading followed by unloaded recovery (**Figure 12**). Following nucleotomy, cyclic loading caused a 7% increase in compressive modulus and a 15% increase in compressive range.[125] In this work, neither the implant nor sham samples altered the cyclic loading effect. Although this process is an important aspect of the disc's *in vivo* diurnal cycle, the effect of a nuclear implant on those compressive properties has not been previously been studied. As a result, it is not known whether other nuclear replacement treatments currently under development preserve cyclic loading effects. As noted above, these responses may be governed more by the annulus fibrosus. It is also possible that the testing frequency of 0.2 Hz did not capture changes in compressive properties that would be more evident at different frequency. In part, this is because the cyclic loading

effects are likely due to fluid distribution within the disc, and the rate at which redistribution occurs has not been studied extensively. Also, one of the primary mechanical functions of the intervertebral disc is to absorb energy, and this damping capacity would be affected by testing frequency. In future studies, it would be interesting to evaluate how the mechanical response of the intact, nucleotomy, and treated discs in various frequencies.

Maintaining disc mechanical properties represents a significant improvement over current surgical procedures, which do not maintain or restore native disc mechanical behavior.[38; 56; 91] In addition, *in situ* curable nucleus pulposus implants, such as this hydrogel, mimic native nucleus function by creating more uniform stress distributions within the disc than other surgical implants.[33] By mimicking native function, the implants may prevent additional damage to the annulus fibrosus. Also, these injectable implants are less invasive than conventional surgeries. This is of particular importance given that repair and regeneration within the disc is limited because of its avascular nature and low cell content.[78; 140] Finally, treatment with an injectable implant does not preclude future surgical alternatives.[33]

Unexpectedly, the hydrogel implant did not restore compressive strain in the human discs (**Figure 14B**), despite restoring compressive strain when implanted in ovine discs.[80] This difference may be attributed to a combination of factors, including the degenerate human annular tissue, the annular nucleotomy injury, and the quantity of hydrogel injected. The human discs used in this study are more

degenerate than the ovine discs used in the previous study in which compressive range of motion was restored.[80] As a result, the hydrogel implant may have been less beneficial because the surrounding tissue already had degraded mechanical properties. Also, the nucleotomy incision depressurized the nucleus pulposus, which prevents the implant from functioning in the same manner as the native nucleus. While the nucleotomy injury was required as a negative control for this study, the implant could be delivered with a much smaller injury in clinical practice, thus avoiding disc depressurization. Finally, in the previous ovine study a greater than 1:1 ratio of implant to nucleotomy volume was delivered. Here however, there was a reduced amount of implant (0.5 mL) compared to nucleus pulposus removed (1.7 mL), a less than 1:3 implant to nucleotomy ratio. This may have prevented some of the beneficial effects of the hydrogel implant. This reduced implant amount may have occurred because samples underwent three periods of overnight hydration in PBS between the nucleotomy procedure and treatment injection. The nucleus pulposus has been shown to swell up to 200% or more in its initial volume.[60] As a result, the remaining nucleus tissue may have expanded to partially fill to nucleotomy void prior to receiving the implant. The hydration steps between nucleotomy and treatment were necessary for this study to establish the nucleotomy samples as an injured control. However, those steps are unique to this study, and in future implementation of the hydrogel, the implant will be placed immediately following nucleotomy.

While implant retention is a significant biomechanical benchmark, it is also encouraging regarding the broader goal of using an injectable hydrogel as a restorative therapy for treating disc degeneration. Bench tests in this gel and others have shown that MSCs within hydrogels can differentiate along a chondrogenic lineage, with aggrecan and collagen production.[72; 128] MSCs embedded in a hydrogel maintained metabolic activity 7 days after injection into porcine discs.[106] The interdigitation of the current hydrogel with the surrounding disc tissue provides interface for collagen, aggrecan, and other extra-cellular matrix components produced by MSCs coinjected with an implant to interact with and reinforce the remaining disc tissue. This reinforcement is an important aspect of establishing hydrogel implants as a restorative therapy for treating disc degeneration and will be the focus of future work.

Previous work on the hydrogel implant has shown that it has properties similar to native nucleus pulposus, can restore compressive range of motion in ovine discs, is biocompatible, promotes cell proliferation, and has the potential to incorporate pharmaceuticals.[32; 80; 128] This chapter expands on those findings by showing that the implant interdigitates with the surrounding disc tissue and was not expelled during 10,000 cycles of compressive loading and preserves disc creep within human L5-S1 discs. These experimental findings provides a solid foundation for continuing to evaluate the efficacy of the hydrogel implant to functionally regenerate the nucleus pulposus.

CHAPTER 5: CREATION OF DISC STRAIN TEMPLATE

5.1 Introduction

As has been mentioned previously, the intervertebral disc supports significant loads while simultaneously permitting spinal mobility. However, injury and degeneration alter disc structure and composition, which in turn affects disc function and the motion of the surrounding spinal column. Tissue strain is an important indicator of mechanical function in load-bearing joints such as the intervertebral disc. Internal disc strains can be used to study healthy disc function and degeneration, to identify injurious loading conditions, and to design and evaluate therapeutic interventions.

The disc's structure of a pressurized gelatinous nucleus pulposus surrounded by the layered fiber reinforced tissue of the annulus fibrosus hinders direct measurement of internal disc strain. The earliest experiments measuring internal disc strain relied on invasive methods such as bisecting the disc or tracking markers inserted within the disc.[88; 89; 120] However, because invasive methods cause structural modifications that inherently alter strain, these measurements may not accurately reflect the native tissue strains. To overcome these difficulties, a number of recent studies have used magnetic resonance imaging (MRI) to non-invasively measure internal deformation under static load.[18; 30; 45; 102] These studies have measured internal strain in two dimensions limited to a plane of interest, typically a mid-coronal, sagittal, or axial plane. This method, while non-invasive, may be

limited due to out-of-plane motion during loading. Moreover, to date these studies have not captured strain in the damage-prone regions of the disc, such as the posterolateral annulus fibrosus.[142] To address these challenges, we recently used ultra-high field MRI and image registration to measure three dimensional internal strain of human intervertebral discs undergoing static axial compression.[157] MR images were acquired with 0.3 mm isotropic resolution and the resulting strain maps provide unparalleled definition of the internal mechanical response of the disc.

The large amounts of data provided and the variability between individual discs in the 3D data set has made discerning group-relevant trends difficult.[157] Within the field of neuroimaging, the challenge of individual variation is addressed by using data from several individuals to create templates, which are essentially averages of the imaging data.[36; 69; 108; 141; 155; 158] These templates may be single-modality, meaning that they are derived from a single imaging source, or they may be multi-modality, by utilizing information from multiple sources such as standard MRI and Diffusion Tensor Imaging.[11; 75] Because templates minimize individual variation in order to highlight key population traits, they are ideally suited for analyzing the recently acquired 3D disc images and strain maps.

Finite element models (FEMs) are ideal for validating the disc strain template method because they are regularly used to examine the entire disc stress-strain profile.[99; 100; 111; 119] We recently created a biphasic disc FEM using the average geometry of L4-L5 disc and region specific tissue properties obtained from a wide

range of experiments.[34; 62] This FEM was validated by comparing its calculated disc-level mechanical response to experimental compressive slow loading ramp, creep, and stress-relaxation tests. Because this model has undergone rigorous validation of the disc's nonlinear compression response, it is well suited for comparison to a template of MRI calculated internal strains. The objective of this study was to use previously acquired 3D MRI strain data[157] to create an internal disc strain template based on a sample set of discs undergoing physiologically relevant compressive loading. We hypothesized that strains would be highest in the posterolateral and posterior regions of the disc. For validation of the strain template technique, template results were compared to a recently created finite element model.[62] Creating a 3D internal disc strain template marks significant progress towards quantifying internal disc strains, which in turn can be used to study normal and degenerate disc function and to design and evaluate therapeutic interventions.

5.2 Methods

5.2.1 Template Creation Overview

The disc strain template was created using a process similar to multi-modality templates.[11; 28] First, multiple MR images of the disc and corresponding strain maps were acquired (**Figure 16A**). Next, a disc anatomical template was created using the MR images (**Figure 16B**). During that process, the transformations (T_1, T_2, …, T_n) between the individual discs and the anatomical template were calculated. Those transformations were used to map the sample strains to the template space (**Figure 16C**). Finally, the transformed sample strains

were averaged to create the disc strain template. In this study, these steps were completed using three dimensional images, strain maps, and transformations. The template creation process is described in more detail below.

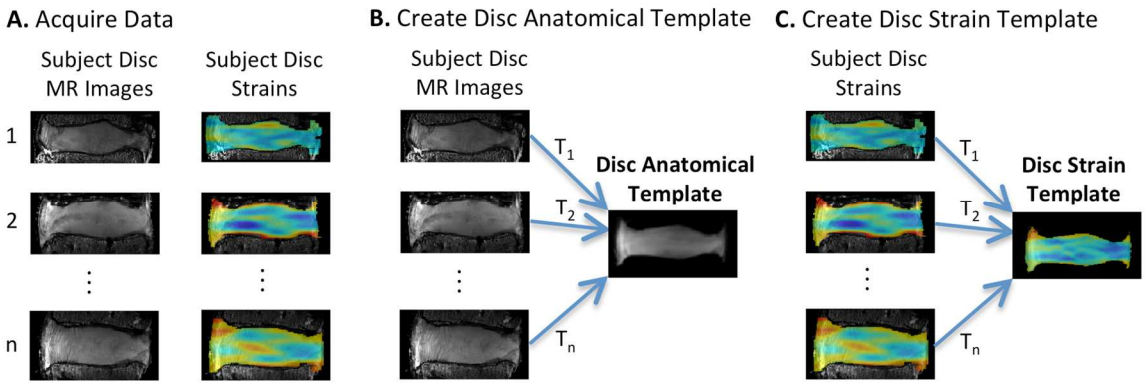

Figure 16: Disc strain template creation process. First, MR images of individual discs are acquired and subject strain maps are calculated (A). Next, the MR images are used to create a disc anatomical template (B). The transforms from the subject discs to the template are saved (T_1, T_2, …, T_n). Those transforms are used to map the subject disc strains to the template space, which are then averaged to create the disc strain template (C). Although images shown are two dimensional, the process is identical in three dimensions.

5.2.2 Data Acquisition

Internal three-dimensional strains maps were recently created for seven grade III human L4-L5 discs (**Figure 16A**).[157] In that experiment, bone-disc-bone samples were prepared by removing the posterior elements and then potting the samples in PMMA. For testing, a sample was placed in a loading rig and 50N of axial compression was applied using a servohydraulic tester (Instron 8874, Norwood, MA) to prevent overhydration. The loading rig was then used to fix the displacement and to transfer the sample to a 7T whole-body MR scanner (Magnetom, Siemens Medical Solutions, Malvern, PA) and imaged. Three-dimensional images with 0.3

mm isotropic resolution were acquired with a sequence designed to enhance lamellar contrast (Turbo Spin Echo, TR/TE = 3000/34 ms, ETL = 7). After imaging, the sample was loaded to -3.6 ± 1.5% axial strain for 3 hours, after which the resulting displacement was fixed and the sample was reimaged using the same parameters. The sample was then loaded and imaged at -7.1 ± 2.9% and -10.3 ± 3.5% strain. Only experimental data acquired in the preload (50N) and -10.3 ± 3.5% steps were used to create the disc template and in this study are refered to as the reference and loaded images, respectively. Peak stress as a result of the -10.3 ± 3.5% applied strain was 0.35 ± 0.22 MPa, which is comparable to the stresses experienced in a wide range of daily activities such as sitting, walking, and climbing stairs.[153]

Strain within the annulus fibrosus was calculated by using Advanced Normalization Tools (ANTs) to register the reference and loaded images.[12; 95; 136] Due to the lack of contrast within the nucleus pulposus region and because of decreasing signal-to-noise ratio with distance from the RF coil, strain was only calculated in the two-thirds of the annulus fibrosus facing the coil. In the original experiment, samples were imaged with either the left or right lateral side facing the coil. To create the template, images acquired with the right lateral side of the disc facing the coil were flipped. This was done for three of the seven image and strain sets used so that the regions of high signal intensity were matched between all seven data sets.

5.2.3 Disc Anatomical Template

From each reference image, the disc was manually segmented from the bone and image background using ITK-Snap.[159] The disc-only images were then used to create a disc anatomical template using an optimization algorithm in ANTs (**Figure 16B**). The algorithm iteratively adjusted the template shape with the objective of minimizing the magnitude of the transformations between the sample discs and the template. The transformations were diffeomorphic, which means they were smooth, differentiable, and invertible.

Transform quality between samples to the anatomical template was assessed using a segmentation image (**Figure 17A**). A segmentation image of each sample was created by manually selecting five annular regions. Next, the segmentation image was placed over the disc anatomical template to visualize the difference between the sample and the template. The segmentation image was then transformed to the template space using the transform calculated between the sample image and the template. The transformed segmentation image was qualitatively assessed to determine if the annular regions of the sample corresponded to the appropriate regions of the template.

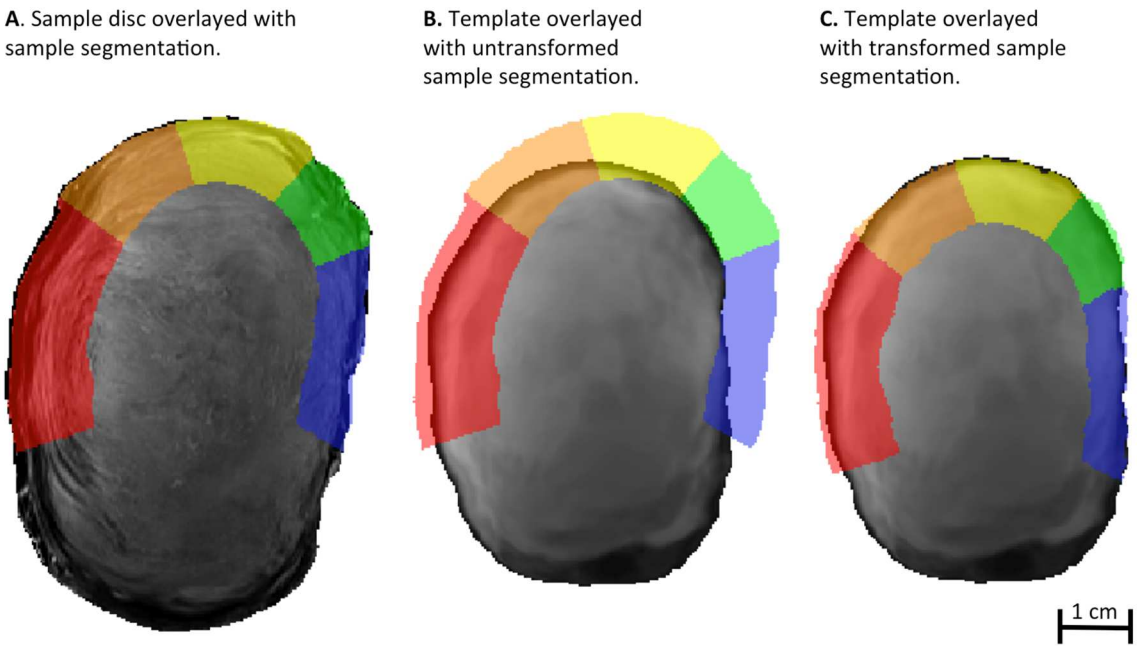

Figure 17: (A) A segmentation image (colored) overlays one of the individual disc images (grayscale) used to create the template. (B) The same segmentation from (A) overlays template, demonstrating that the individual disc is notably larger than the template. (C) The individual disc segmentation is transformed to the template. The transformed mask matches the outer contour of the template and original features of the original mask are preserved, including the diagonal lines between the annular regions, indicating a reasonable transformation between the individual disc and the template.

5.2.4 Disc Strain Template

The disc strain template was created by first expressing the sample strain tensors in an anatomical coordinate system consisting of three orthogonal basis vectors: axial vectors perpendicular to the midaxial slice, circumferential vectors parallel with the outer disc contour, and radial vectors perpendicular to the outer disc contour (**Figure 18**).[157] Strain components of each sample were then transformed to template space using the transformations between each sample and the disc anatomical template. Because the strain tensors were expressed in terms of

local coordinates, vector orientation relative to disc anatomy was preserved during transformation. The transformed strain components were averaged to create the disc strain template.

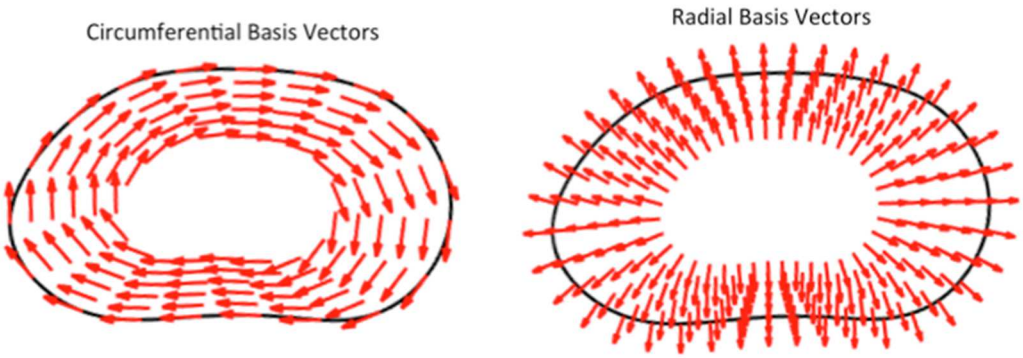

Figure 18: Circumferential and radial basis vectors for a local disc coordinate system. Defining the strain in local coordinate system facilitates transformation of strain tensors from the subjects to the template.

The template's effectiveness in achieving the objective of reducing individual variability in strain maps while preserving general trends was evaluated using the first invariant of the Lagrangian strain tensor. The first invariant is a scalar that is independent of coordinate system and represents the average deformation at that point. Invariant maps were created for each sample and for the template. Then, the invariant template was qualitatively examined to determine if the specimen-specific peaks had been reduced while preserving the general trend of a higher invariant in the posterior region.

5.2.5 Regional Strain Analysis

Disc strain was analyzed as a function of anatomic location. The annulus fibrosus was partitioned into five regions of interest: anterior, anterolateral, lateral,

posterolateral, and posterior (**Figure 19A**). To evaluate the difference between the inner and outer annulus, the five regions were divided in half. To avoid bone-disc interface effects, data was analyzed in the mid-third of the disc height (**Figure 19B&C**).

Each voxel of the strain template represents data for seven individual discs spatially normalized to the same anatomical location. For plotting purposes, the mean strain was calculated at each voxel, and boxplot and overlay images were created using the voxel means within the region of interest. For statistical analysis, the mean strain in each annular region was calculated for each of the transformed sample discs. The differences in region means of the seven samples were then evaluated using a repeated measure ANOVA with a Holm-Sidak Multiple Comparison Test. Significance for all tests was set at $p < 0.05$.

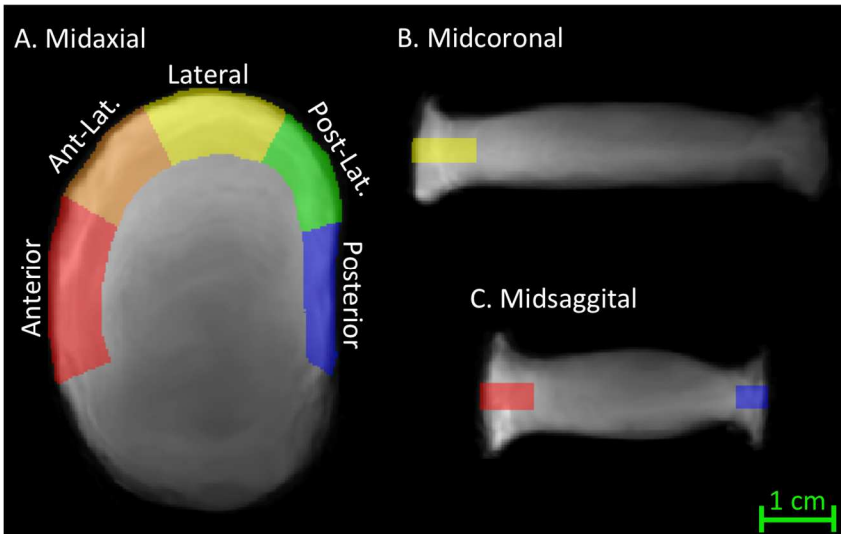

Figure 19: Midaxial (A), midcoronal (B), and midsaggital (C) slices of the disc anatomical template. The annulus of approximately the mid-third of axial region of the disc was divided into five regions: anterior, anterolateral, lateral, posterolateral, and posterior. The right side of the template was more poorly defined than the left, because the original images had lower signal-to-noise and contrast-to-noise ratios in the right side.

5.2.6 Comparison to Finite Element Model

Both the finite element model and the anatomical template are average shapes of human L4-L5 discs. However, the finite element model used principal component analysis of an independent set of L4-L5 disc images to define the model geometry. As geometry affects FEM results,[100] the shapes of the disc anatomical template and the finite element model were compared before comparing the FEM strain results with the strain template.

The internal results of a recently validated biphasic FEM[62] of the intervertebral disc were compared to the strain template. After simulating the same loading conditions as the samples used to create the same template, the finite element model strain results were sampled to match the template voxel distribution. The finite element model was then registered to the template, so that each voxel of the strain template corresponded to a voxel representing FEM results. At each voxel, the mean and standard deviation of the transformed sample disc strains was compared with the FEM results. Because there was no standard deviation associated with the finite element measurements, no statistical tests were performed. Instead, the difference between the FEM result and template mean strain was compared in terms of the template standard deviation.

5.3 Results

5.3.1 Disc Anatomical Template

The final disc anatomical template held the expected shape of an intervertebral disc (**Figure 19**). Total computational time to create the anatomical template was 10 hours, with 30 seconds for the first step, 0.5 hours for the second, 1.5 hours for the third, and 8 hours for the final step while using seven Intel Xeon compute cores. The most striking difference between the original images and the template is the darker and less defined edges of the right side of the disc (**Figure 19B**). However, this lack of edge definition was expected given the lower contrast on the right side of the disc in the original images. Also, the template lacked lamellar contrast. Again, this was expected because the template is an average of multiple discs.

Importantly, labels transformed from the samples to the template matched the expected areas well (**Figure 17**). The disc shown in **Figure 17**A had the largest cross-sectional area of the sample set, and hence the transformation between the sample and the template was larger than that of most of the other samples. Irrespective of the difference between each sample and the template, the general features of the sample labels are appropriately transformed to the template. Specifically, after transformation the outer contour of the discs match, the relative thickness of the annulus is similar, the inner boundary of the annulus remains smooth, the boundaries between the five annular regions remain diagonal lines, and the five annular regions match the appropriate location in the template. This

indicates that locations in the individual discs correspond to the appropriate anatomic location on the template, and this successful spatial normalization allows for the creation of the disc strain template.

5.3.2 Disc Strain Template

The invariant of the deformation tensor for the individual samples was consistently higher in the posterior and lateral regions of the discs compared to the anterior regions (**Figure 20**). However, there was also considerable variation in the magnitude of invariants between samples and the location of the peak invariants. The strain template notably reduced individual peaks evident in the invariants of the individual discs. It also preserved the pattern of higher values in the posterior region.

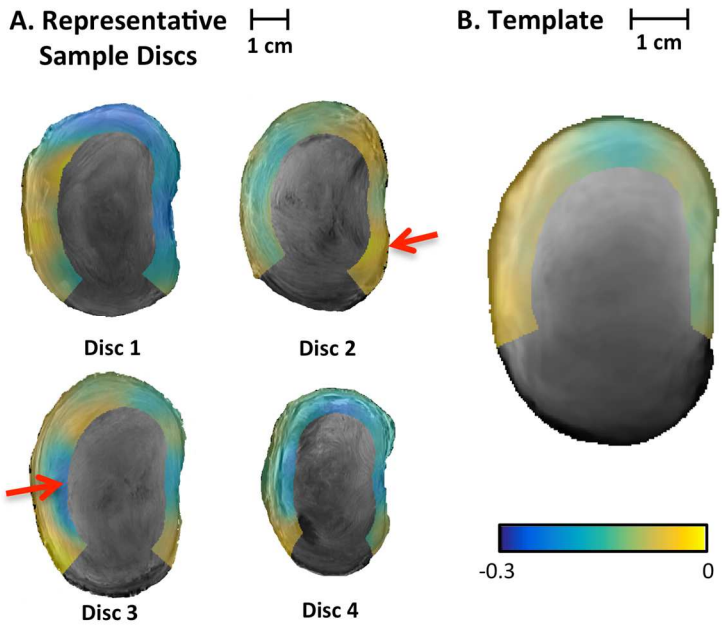

Figure 20: Midaxial disc slices showing the first invariant, a measure of volumetric change, of four of the seven individual discs and the template. The

template does not have the invariant peaks evident in many of the samples (e.g. the peaks located at arrows in Discs 2 and 3). The template preserved general trends, such as higher invariants in the posterior region.

5.3.3 Regional Strain Analysis

Axial strain varied from -6.8% to -22.0% (**Figure 21A**). The magnitude of axial strain was lower in the anterior region (-9.9%) than in the lateral region (-16.6%, $p < 0.05$, **Table 1**). The mean axial strain in the lateral, posterolateral, and posterior regions were similar, with values of -14.3 to -16.6% ($p > 0.2$). The range of circumferential strain (1.4 to 5.3%, **Figure 21B**) was much smaller than the range of axial strain. There was a region of high circumferential strain in the lateral and border of the posterolateral regions of the annulus, although this difference was not statistically significant ($p > 0.2$). In contrast to the axial strain, the circumferential strain component was similar in the anterior and posterior regions ($p > 0.9$). The radial strain components had a slightly larger range (-3.5% to 4.4%, **Figure 21C**) than the circumferential strain. Mean radial strain in the lateral region (-0.5%) was lower than radial strain in the anterior (2.5%), anterolateral (1.4%), posterolateral (2.5%), and posterior (2.8%) regions ($p < 0.05$). Similar to the circumferential strain, radial strain magnitude is similar in the anterior and posterior regions ($p > 0.7$). Between most of the inner and outer annulus regions, the difference in strain components was not significant (**Figure 22**). The notable exception is in the radial strain of the lateral region, with a mean strain of -1.4% in the outer annulus and 1.1% in the inner annulus ($p < 0.1$).

Table 1: Mean (standard deviation) of strain values for the L4-L5 Template in the five annular regions and throughout the annulus fibrosus. A=Anterior, A-L = Anterolateral, L = Lateral, P-L = Posterolateral, and P = Posterior.

	A	**A-L**	**L**	**P-L**	**P**	**Total**
Axial	-9.9(2.0)	-12.7(3.0)	-16.6(2.9)	-14.3(1.7)	-15.8(1.7)	-13.5(3.5)
Circum.	2.3(0.4)	2.2(0.6)	3.8(0.8)	3.0(0.6)	2.3(0.4)	2.7(0.9)
Radial	2.5(0.5)	1.4(1.3)	-0.5(2.0)	2.5(0.9)	2.8(0.9)	1.6(1.8)

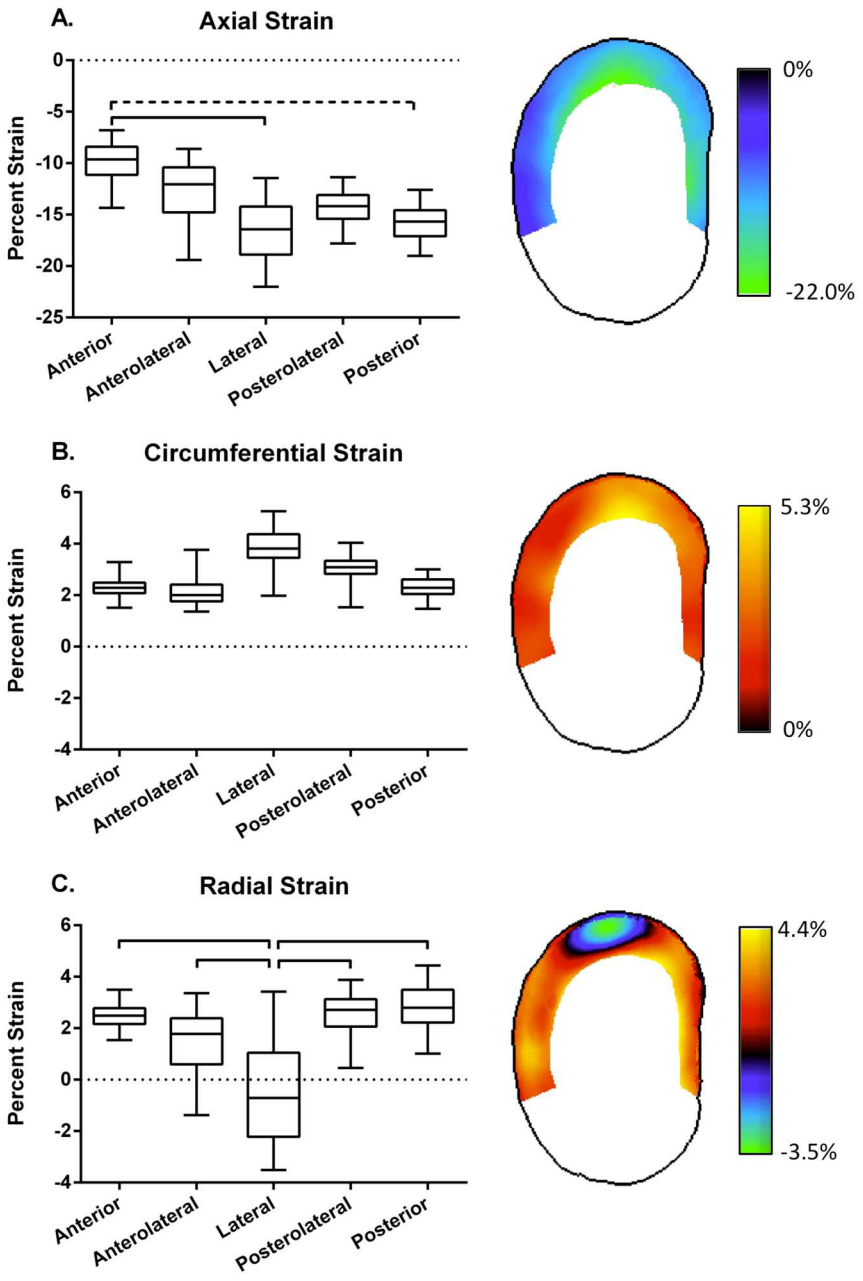

Figure 21: Boxplots of the voxel strain distributions in the five annular regions for the axial (A), circumferential (B), and radial (C) strain components. The data represents the strain component values at each of the voxels within the regions as defined in**Figure 19**. Midaxial slices of the strain template are also shown. Axial strain has a wide range of -6.8% to -22% and is lower in the lateral, posterolateral, and posterior regions. Circumferential strain is highest in the lateral region, while the radial strain is lowest in that region. Solid lines are significant differences between means of the seven subject discs transformed to the template space ($p < 0.05$), and dotted lines are trends ($p < 0.1$).

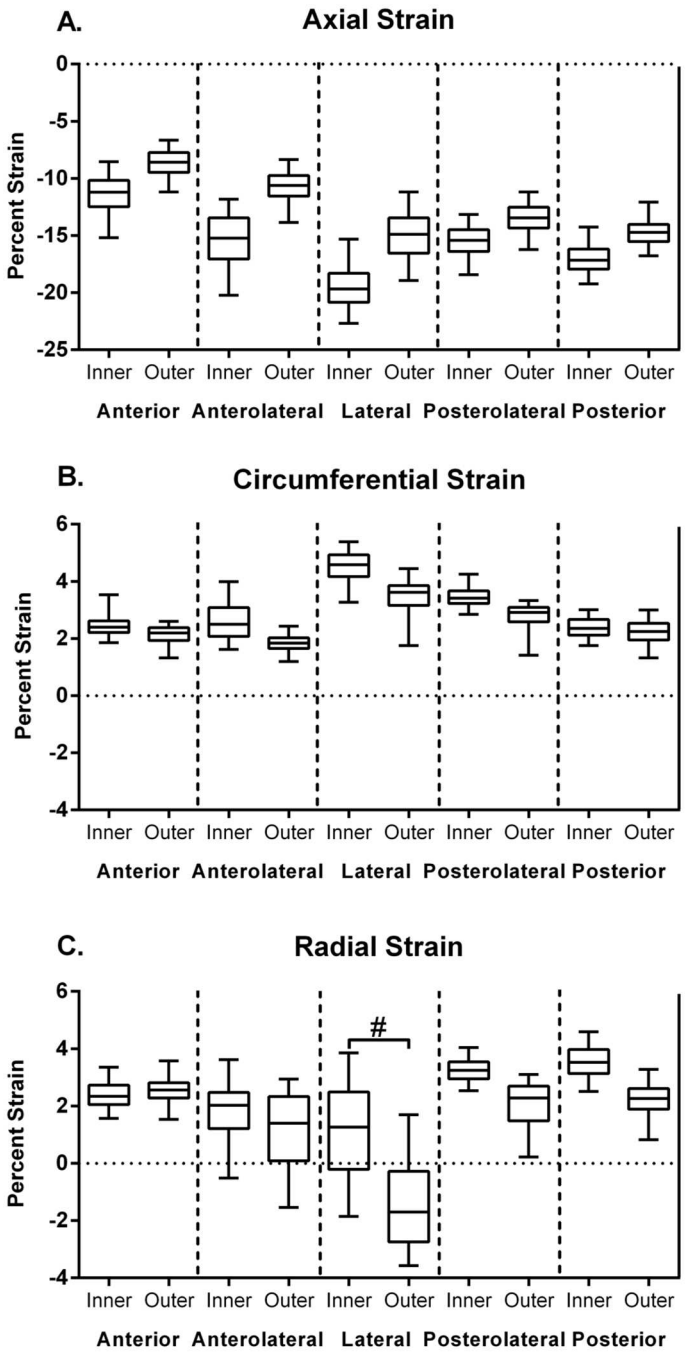

Figure 22: Comparison of voxel distributions of axial (A), circumferential (B), and radial (C) strain components between the inner and outer annulus of the strain template. In most regions, there was minimal difference between the inner and outer annulus. However, the axial component had greater compressive strain in the inner portion of the anterolateral and lateral regions. Similarly, the radial and circumferential strains were higher in the inner lateral region than the outer lateral region. #indicates trend in differences between means of the seven subject discs transformed to the template space ($p < 0.1$).

5.3.4 Comparison to Finite Element Model

The geometry of the FEM and the disc anatomical template were very similar, differing by a few millimeters in disc height, anteroposterior width, and lateral width (**Figure 23**). The contours of the midaxial slices were also very similar. However, the shapes differed in that the disc anatomical template had peaks along the outer rim of the inferior and superior edges that were not present in the FEM geometry. The difference between profiles is probably due to the different imaging sequences used to acquire the FEM and template data sets. The FEM data set was acquired using a 3D fast low-angle shot (FLASH) sequence,[108] while the template data set was acquired using a 3D turbo spin echo sequence. In the FLASH sequence, the outer rim of the disc was not visible, and hence was lacking in the FEM shape.

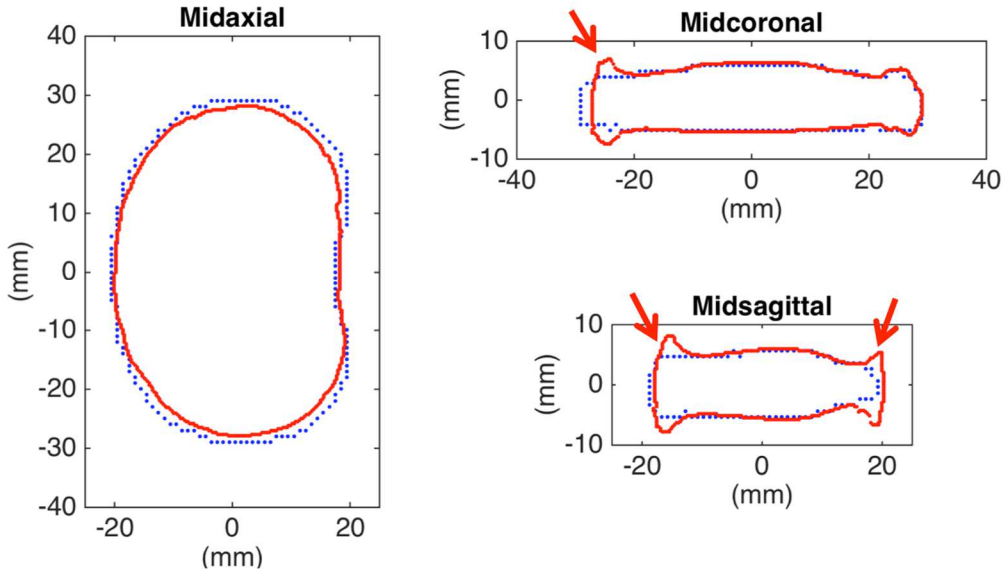

Figure 23: Comparison of the disc template created in this study (red) and the finite element model geometry (blue), which were created using different samples and methods.[108] The template and shape model are similar in both shape and size. The shapes differed in that the disc anatomical template had peaks along the outer rim of the inferior and superior edges that were not evident in the FEM geometry (see arrows in midcoronal and midsagittal views).

The FEM internal strains were similar in magnitude to the disc strain template (**Figure 24A&B**). The finite element results were within one standard deviation of the template values for 85.5%, 99.5%, and 81.4% of all voxels for the axial, circumferential, and radial strain components, respectively (**Figure 24C**). The areas of largest difference were in the anterolateral and lateral regions for the axial strain component and the posterior region of the radial strain component. These differences are also evident in the distribution of template mean strains and the finite element results (**Fig. 10**). The measured template axial strain was 4.2-6.0% strain lower than the calculated values of the FEM in the anterolateral and lateral regions of the disc (**Figure 25A**). The circumferential strain was 1.0-1.5% strain higher in the template than the finite element model in the lateral, posterolateral, and posterior regions (**Figure 25B**). The radial strains in the template were also 2.0% strain lower than the FEM in the lateral region and 3.8% strain lower in the posterior region (**Figure 25C**). Of the fifteen comparisons between the template and the FEM (3 strain components and 5 regions), the difference in medians between the two was less than 2.5% strain for all but three of the comparisons.

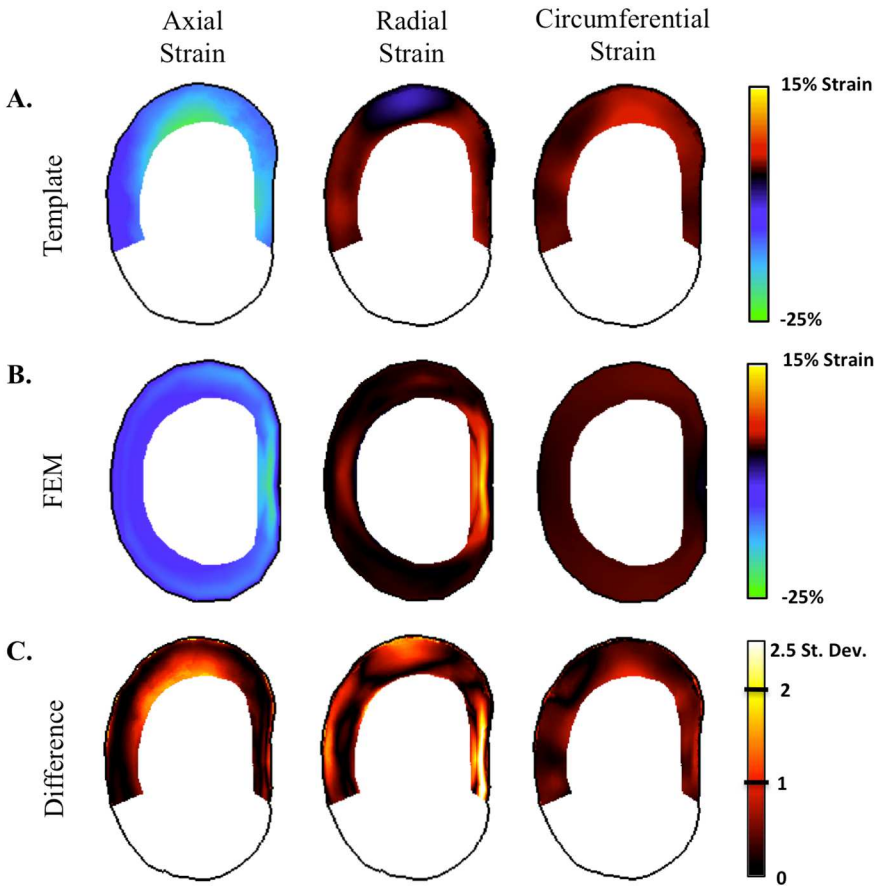

Figure 24: Midaxial slices of the strain template (A) and finite element model (B). The difference of the FEM from the template mean is also shown in terms of the standard deviation at each voxel (C). The strains predicted by the FEM are within 1 standard deviation for the majority of the annulus in all three strain components. The greatest difference between the FEM and template is the peak radial strains in the posterior region.

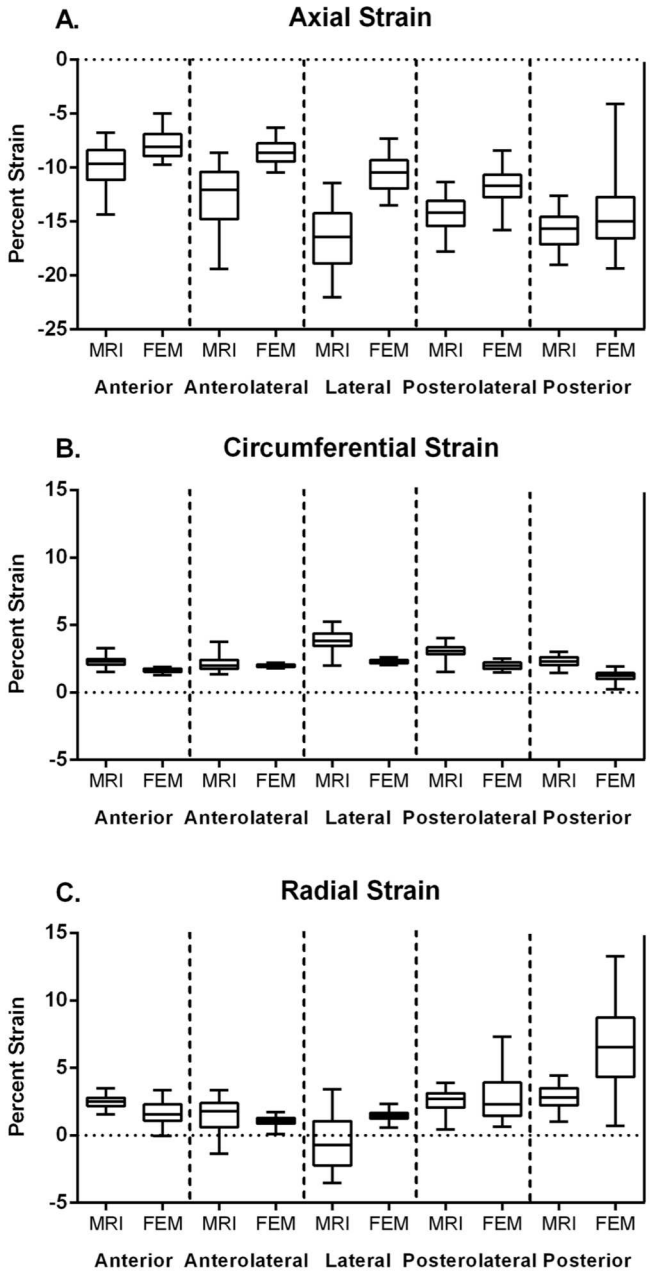

Figure 25: Comparison of template strains and finite element model strains in the mid-third of the disc. Median strains between the template and finite element model are within 0.2-2.5% strain for all compared regions except for the axial component in the anterolateral and lateral regions and the radial component in the posterior region.

5.4 Discussion

This chapter successfully completed the objective of creating an internal disc strain template for human L4-L5 discs undergoing a physiologically relevant compressive load. The individual strain maps contained 3D strain data that was measured non-invasively. As expected, the combination of 3D maps from individual discs into a single template reduced individual variability to allow for the study of group-level trends in local 3D strain such as high compression strain in the posterolateral and posterior regions (**Figure 20**). These trends were validated by comparison to the internal strains calculated by a finite element model. Creating the strain template is a substantial improvement in studying internal disc mechanics and provides a new methodology useful for multiple studies, such as studying the effect that disc degeneration and treatments have on internal disc strain.

The strain distributions of the template can be interpreted within the context of disc anatomy. Because the loading was axial compression, axial strains were much greater in magnitude (-7 to -22%) than circumferential and radial strains (-3.5 to 5.5%), which is consistent with the compression load causing an internal pressure that subsequently pushes the annulus outward. The amount of bulging as measured by mean radial strain is consistent with 2D MR strain measurements (1.8% vs 2.1% strain).[101] Axial strain was greater in the posterior, posterolateral, and lateral regions of the disc than the anterior region (**Figure 21A**). Also, circumferential strain was highest in the lateral and posterolateral regions of the disc (**Figure 21B**). In conjunction with the thinner annulus in the posterior and

posterolateral region, this may explain why there is a higher occurrence of radial tears in the posterolateral region.[142] Also, in the region with the highest circumferential strain (lateral), the radial strain was compressive, which is a consistent with a normal Poisson's effect. It is interesting to note that in most disc regions, the strains of the inner and outer annulus were not different (**Figure 22**). The notable exception is the lateral region, in which the inner annulus had greater strain magnitudes. This difference between inner and outer annulus could be due to several factors, including the higher curvature of the disc in that region, the lower disc height over the inner annulus than outer annulus, and potentially different mechanical properties between the inner and outer annulus.[34; 50] However, the continuum of structure and composition from outer to inner annulus makes it difficult to distinctly separate these regions.

The wide range of observed axial strain magnitudes highlights the inhomogeneity created by the disc's structure and composition. The mean measured axial strain is comparable to the applied strain of -10.3 ± 3.5%, but the range of -6.8% to -22.0% is substantial. The circumferential and radial strain components also had wide ranges of 1.4 to 5.3% and -3.5 to 4.4%, respectively. Thus, even in a very simple loading condition that is representative of daily activities such as sitting and walking,[153; 157] there are regions of the disc's structure that experience high strains that may eventually lead to tissue damage. The wide range is also important to consider in the context of the disc's cellular environment. Strain is attenuated between the tissue and cellular levels of fibrous tissue, including the intervertebral

disc.[49; 133; 137] However, the magnitude of measured strain in this work indicate that even with attenuation in a simple loading condition the cells that inhabit the disc experience a varied mechanical environment with the potential to influence cellular function.

The majority of the strain template results were consistent with the FEM. For example, in both methods the highest circumferential strain was in the lateral region with a corresponding minimum of radial strain (**Figure 23B & C**). Overall, the FEM results were within one standard deviation for over 80% of the regions examined (**Figure 24C**). This high level of agreement gives confidence that the template internal strain measurements for a disc undergoing axial compression are reasonable.

While the strain template was compared to the finite element model to ensure that the template results were reasonable compared to a widely accepted method of evaluating internal strains, the experimentally derived template can also serve as an internal validation of the finite element model. Finite element models are valuable tools in evaluating a disc's mechanical function because they have the ability to rapidly evaluate the effects of more complex loading conditions and to perform experiments altering properties that are not feasible to adjust in physical experiments. Unfortunately, disc FEMs are often constructed with significant assumptions concerning internal structure and mechanical properties, such as disc geometry, tissue constitutive models, viscoelasticity, collagen fiber angle, and material properties of the tissue structures. Furthermore, they are routinely

validated using only simple, and often single, global parameters such as the amount of height loss during compression. As a result, the validity of the disc FEM results is of concern and the suitability to use internal outputs has not been evaluated.

The finite element model examined in this study had already gone through extensive validation of geometry, material model selection, and of the non-linear response to compressive loads.[62] Despite the extensive validation of the finite element model, the comparison to the strain template uncovered two regions where the FEM did not match the measured results: the axial strains in the anterolateral region and the radial strains in the posterior region (**Figure 24C** & **Figure 25**). The peak radial strains in the posterior region are possibly due to the rectangular, rather than cube, shape elements in the region that may cause small discontinuities in fiber distribution within the model. The difference between the FEM and template axial strain may be due to the difference in the superior and inferior vertebral edges between the template and FEM (**Figure 23**). Note that these differences did not cause discrepancies in the extensive testing and validation of the nonlinear disc-level mechanical response of this finite element model,[62] indicating that care should be taken in using internal outputs of finite element models that have been validated using disc-level parameters. However, despite the need for further refinements to the model, the mean predictions of the current FEM and template were similar in most respects.

While the purpose of creating the template was to eliminate individual variation in order to highlight group trends, the template can also be used to

examine individual variations. Studying individual variations can be done by comparing and contrasting the strain distributions of an individual disc with the template strain map. This is important, because peak strains present in individual discs may be indications of local tissue damage, similar to the way in which contact stress peaks individual hip joints are likely the cause of pain.[51] By using a template to establish normal strain patterns, individual deviations can be more readily identified.

In conclusion, the disc strain template provides an unprecedented view of the internal intervertebral disc strain. The combination of multiple 3D maps into a single template allows for the study of general strain trends within the disc. The comparison between the template strains and finite element model indicate that the template strains are reasonable and demonstrate a need for validating the internal strains calculated by finite element model. Studying tissue strain by using templates is a technique that is readily applicable for use in other joints and tissues. Moreover, the technique provides a new methodology useful for a wide range of studies, including more complex loading conditions, comparison of individual disc strain with the template strains, the effects of disc pathologies and degeneration, damage mechanisms, and design and evaluation of treatments.

CHAPTER 6: EFFECT OF NUCLEOTOMY ON INTERNAL DISC STRAIN

6.1 Introduction

As described in chapter 3, nucleotomy alters disc mechanics by decreasing disc height, NP pressure, and stiffness while increasing range of motion and creep.[21; 25; 42; 46; 61; 88; 104] A two-dimensional study of the effect of nucleotomy on internal strains found that the increased compressive disc strain translated to higher axial strains within the disc and altered distributions in radial strain between the anterior and posterior regions.[104] Because of the two-dimensional nature of the study, circumferential strains, which would tend to cause annular tears, were not measured. Also, measurements were limited to the midsagittal and midcoronal planes.

The objective of the current chapter is to measure the effect of nucleotomy on the internal strains of mildly-degenerate human discs. This was done using the strain template technique developed in chapter 5, which allows for the comparison of the 3D strain components throughout annulus fibrosus.

6.2 Methods

6.2.1 Data Acquisition

Twelve human grade II L3-L4 bone-disc-bone samples were prepared in the manner described in section 5.2.2. Five of the 12 samples had significant imaging

artifacts and were eliminated from the study. Each of the seven remaining samples was tested in a similar manner to the data acquisition process described in chapter 5. Testing began by hydrating the sample overnight in a refrigerated PBS bath. Next, the sample was placed in the loading rig[157] and 30N axial compression load was applied using an Instron ElectroPuls (E3000, Instron, Norwood, MA) to overcome the overhydration that results from the overnight hydration. Afterwards, the sample was transferred to and imaged in a 7T MR scanner (Magnetom, Siemens Medical Solutions, Malvern, PA) with 0.3 mm isotropic resolution. After imaging, the sample was loaded to -9.5 ± 3.2% axial strain for 3 hours, after which the resulting displacement was fixed and the sample was reimaged. Samples were frozen following imaging. Unlike the previous data set, no images were taken at intermediate strain values. Peak stress as a result of the -9.5 ± 3.2% applied strain was 0.71 ± 0.23 MPa, which is comparable to the stresses experienced in a wide range of daily activities such as standing, jogging, and climbing stairs.[153] Equilibrium stress after three hours of -9.5% applied strain was 0.22 ± 0.08 MPa.

After intact loading and imaging were complete, 1.1±0.4 g of nuclear material was removed (approximately 30% of nucleus volume[27; 39]) as described in section 3.2.3 and samples were subsequently returned to the freezer. Samples lost 0.6 mm of disc height as a result of nucleotomy.

Nucleotomy testing and imaging were identical to intact testing and imaging, except that samples were loaded to 0.71±0.23 MPa to match the resultant loads of the intact test. Applied stress was matched during testing rather than the applied

strain because samples lost disc height as a result of nucleotomy, thereby altering the initial height used to calculated applied strain. 13.4±3.7% compressive strain was applied to the nucleotomy samples as a result of the 0.71±0.23 MPa applied stress. Equilibrium stress for samples following nucleotomy was 0.18 ± 0.06 MPa.

6.2.2 Anatomical and Strain Template Creation

Strain maps were calculated for each of the unloaded and loaded image pairs by first creating bone-disc-bone segmentations of the images in ITK-SNAP[159] as described in section 5.2. The segmented images were registered using ANTs. Strain tensors were then calculated from the transformation found in the registration process.

Intact and Nucleotomy disc anatomical templates were created using disc only segmentations of the unloaded images as described in 5.2.3. Computational time to create each anatomical template was approximately 11 hours using 7 Intel Xeon compute cores, which is similar to the time used to create the L4-L5 disc anatomical template in chapter 5. The outer contour of the anatomical template of the intact L3-L4 disc was compared with the L4-L5 template developed in chapter 5.

After the anatomical templates were created, the intact strain template was created by transforming the seven intact strain maps to the intact template space. Similarly, the nucleotomy strain template was created by transforming the seven nucleotomy strain maps to the nucleotomy template space. After transformation to the appropriate template space, sample strain components were averaged to create strain templates.

6.2.3 Intact Strain Analysis

Similar to the regional strain analysis of the L4-L5 template in chapter 5, disc strain was analyzed as a function of anatomic location. The annulus fibrosus was partitioned into five regions of interest: anterior, anterolateral, lateral, posterolateral, and posterior (**Figure 26A**). To avoid edge effects, the superior and inferior bone-disc boundaries were excluded from analysis (**Figure 26B&C**). For statistical analysis, the mean strain in each annular region was calculated for each of the transformed sample strain components. The differences in region means of the seven samples were then evaluated using a repeated measure ANOVA with Holm-Sidak test. Significance for all tests was set at $p < 0.05$.

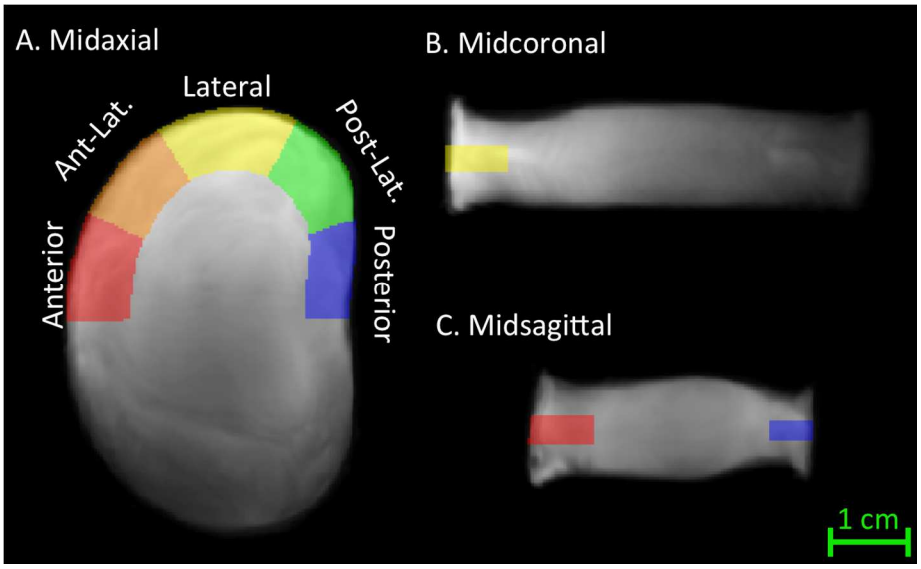

Figure 26: Midaxial (A), midcoronal (B), and midsagittal (C) views of the intact L3-L4 template showing the five annular regions used for strain analysis.

6.2.4 Effect of Nucleotomy on Internal Strain

To determine the effect of nucleotomy on internal strain, mean strains in the five anatomical regions of the nucleotomy were compared as described for the intact template. Also, direct comparison between the intact and nucleotomy templates was completed by first registering the midaxial region of the nucleotomy template to the midaxial region of the intact template. Voxel-wise paired t-tests with a False Discovery Rate were conducted between the intact and nucleotomy values. Significance for all tests was set at $p < 0.05$.

6.3 Results

6.3.1 Anatomical Templates

The intact L3-L4 anatomical template was similar to the L4-L5 template (**Figure 26** and **Figure 27**). The profiles of the superior and inferior surfaces were very similar between the two levels. The two disc shapes were very similar, although the L3-L4 template had a smaller cross-sectional area of 1582 mm^2, compared to 1832 mm^2 for the L4-L5 template. The L3-L4 disc was also slightly taller, with an average disc height of 11.7 mm compared to 10.9 mm for the L4-L5 discs. The L3-L4 disc also had a slight posterior notch corresponding to the vertebral foramen in the axial cross-section that is not evident in the L4-L5 template. The L3-L4 template following nucleotomy was almost identical to the intact L3-L4 template, except that the average disc height decreased by 5% from 11.7 to 11.1 mm.

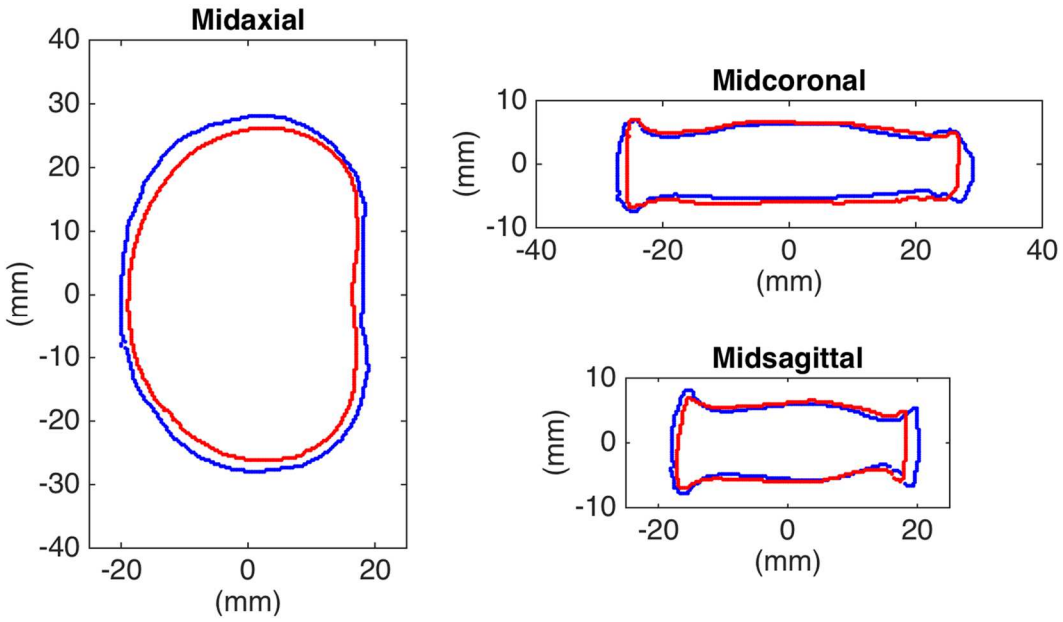

Figure 27: Midaxial, midcoronal, and midsagittal views comparing the L4-L5 (blue) and L3-L4 (red) templates. The two discs shapes are very similar. However, the L3-L4 template has a smaller cross-sectional area and has a slightly larger disc height.

6.3.2 Intact Strain Analysis

In the intact template, axial strain ranged from -2.2% to -25.9% strain (**Figure 28**). Axial strain was highest in the anterior region, with a mean value of -13.8% strain ($p < 0.05$, **Figure 28A, Table 2**). There was no significant difference in axial strain between the means of the other four annular regions, which ranged from -19.6% to -21.0% strain ($p > 0.4$). Circumferential strain varied from 2.3% to 6.9% strain and was lowest in the posterolateral region with a mean of 3.3% strain ($p < 0.05$, **Figure 28B**). There was no difference in circumferential strain between the other four annular regions, which had means of 5.0-5.8% strain ($p > 0.2$). Radial strain ranged from 1.2% to 8.6% strain and was lowest in the lateral region, with a

mean of 3.1% strain, although this difference was not statistically significant (**Figure 28C**). Again, there was no difference in radial strain in the other four annular regions, which had means of 5.4% to 6.0% strain.

Table 2: Mean (standard deviation) of strain values for the Intact L3-L4 Template in the five annular regions and throughout the annulus fibrosus. A=Anterior, A-L = Anterolateral, L = Lateral, P-L = Posterolateral, and P = Posterior.

	A	**A-L**	**L**	**P-L**	**P**	**Total**
Axial	-13.8(5.9)	-19.6(4.7)	-21.0(2.7)	-20.3(2.4)	-21.0(2.7)	-18.8(5.1)
Circum.	5.2(0.8)	5.0(0.7)	5.8(0.9)	3.3(0.6)	5.0(0.8)	5.0(1.1)
Radial	5.4(0.9)	6.0(1.2)	3.1(1.2)	5.6(1.5)	5.5(1.4)	5.0(1.6)

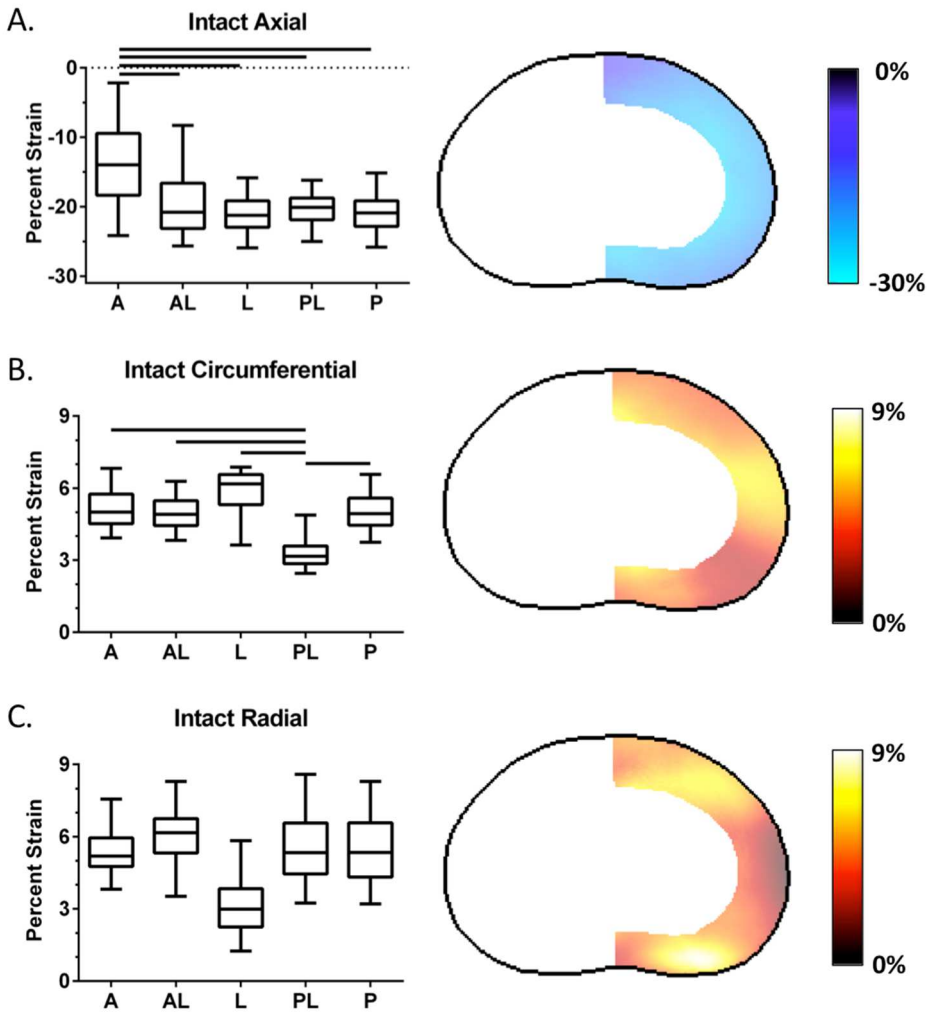

Figure 28: Axial (A), circumferential (B), and radial (C) strain of intact L3-L4 template. Axial strain was highest in the anterior region, circumferential strain was lowest in the posterolateral region, and radial strain was lowest in the lateral region. Solid line: $p < 0.05$

6.3.2 Effect of Nucleotomy on Internal Disc Strain

In the nucleotomy strain template, axial strain ranged from -11.9% to -29.8% strain (**Figure 29**). There was no significant difference in axial strain between the means in the anterolateral, lateral, posterolateral, and posterior regions, which ranged from -24.4% to -26.2% strain ($p > 0.4$, **Figure 29A,**

Table 3). Mean axial strain in the anterior region was -21.5% strain, which was higher than strain in the posterior region ($p < 0.05$). Circumferential strain varied from 2.8% to 6.9% strain, and in contrast to the intact template, there were no differences between regions (**Figure 29B**). Radial strain ranged from 0.6% to 8.9% strain and there were no differences between regions (**Figure 29C**).

Axial strain was lower in the nucleotomy template than in the intact template for all five annular regions, with differences ranging from -0.9% to -12.3% strain (**Figure 30A**). The mean difference in axial strain was -7.6% in the anterior region, and the difference was slightly lower in the other four regions, with difference means ranging from -4.7% to -5.4% strain (**Table 4**). In the nucleotomy template, circumferential strain was 0% to 2.5% lower in the anterior and anterolateral regions compared to the intact template, while it was 0% to 1.5% higher in the posterolateral and lateral regions (**Figure 30B**). Nucleotomy decreased the amount of radial strain in the anterolateral region by an average of -1.5% strain (**Figure 30C**).

Table 3: Mean (standard deviation) of strain values for the Nucleotomy L3-L4 Template in the five annular regions and throughout the annulus fibrosus. A=Anterior, A-L = Anterolateral, L = Lateral, P-L = Posterolateral, and P = Posterior.

	A	A-L	L	P-L	P	Total
Axial	-21.5(4.2)	-24.4(3.1)	-25.7(2.0)	-25.8(2.1)	-26.2(2.5)	-24.4(3.5)
Circum.	3.8(0.6)	4.2(0.2)	5.2(0.4)	4.3(0.4)	5.5(0.7)	4.5(0.8)
Radial	3.8(2.1)	4.5(1.1)	3.7(0.8)	5.8(1.5)	6.1(1.1)	4.6(1.8)

Table 4: Mean (standard deviation) of difference between the strain values of the intact and nucleotomy template in the five annular regions and throughout the annulus fibrosus. Negative values indicate the strain component decreased as a result of nucleotomy. A=Anterior, A-L = Anterolateral, L = Lateral, P-L = Posterolateral, and P = Posterior.

	A	A-L	L	P-L	P	Total
Axial	-7.6(2.9)	-4.8(2.2)	-4.7(1.6)	-5.4(1.3)	-5.2(1.6)	-5.6(2.4)
Circum.	-1.4(0.5)	-0.7(0.5)	-0.6(0.8)	1.0(0.3)	0.4(0.3)	-0.5(1.0)
Radial	-1.6(1.5)	-1.5(0.8)	0.6(0.6)	0.2(0.5)	1.0(1.0)	-0.4(1.4)

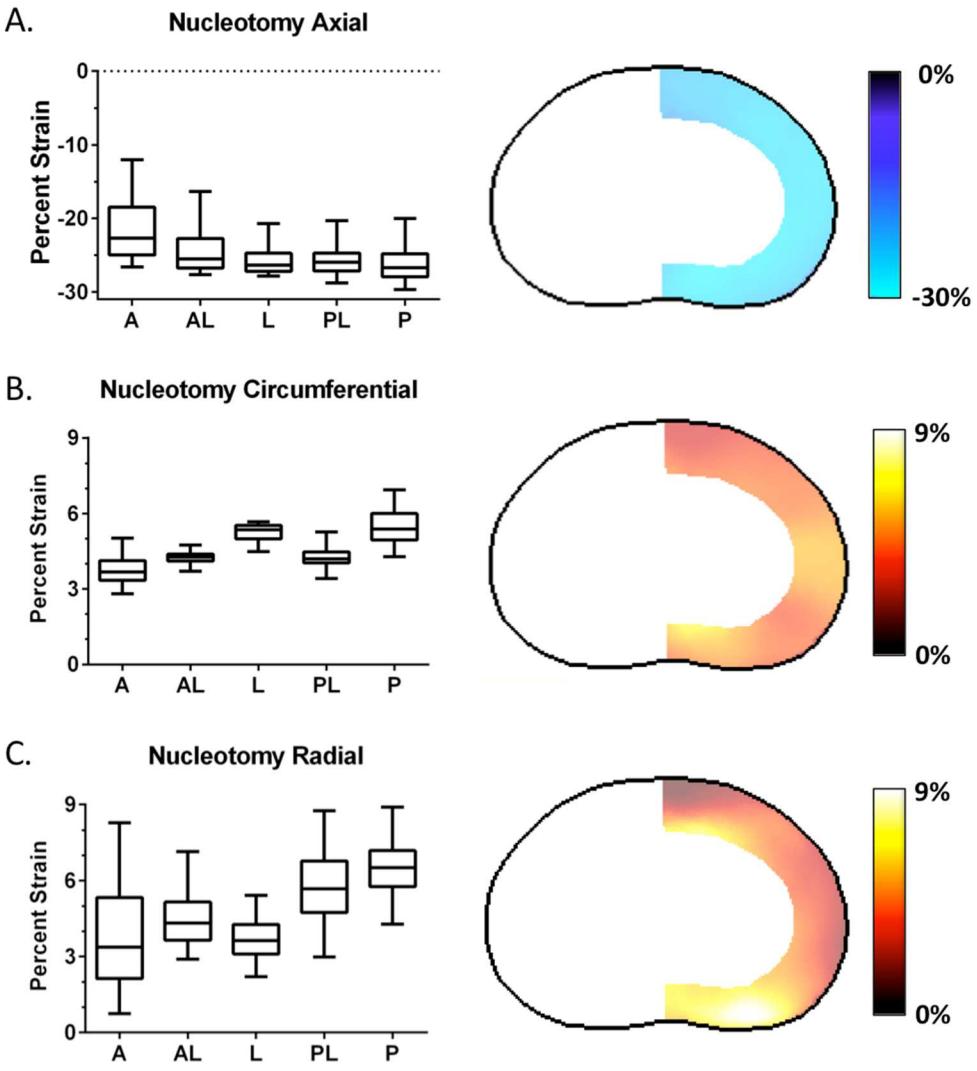

Figure 29: Axial (A), circumferential (B), and radial (C) strain components for the nucleotomy strain template. Mean axial strain was approximately 25% compressive strain in all regions except anterior, which had slightly less compression (A). There were no statistically significant differences in circumferential and radial strain. (B&C).

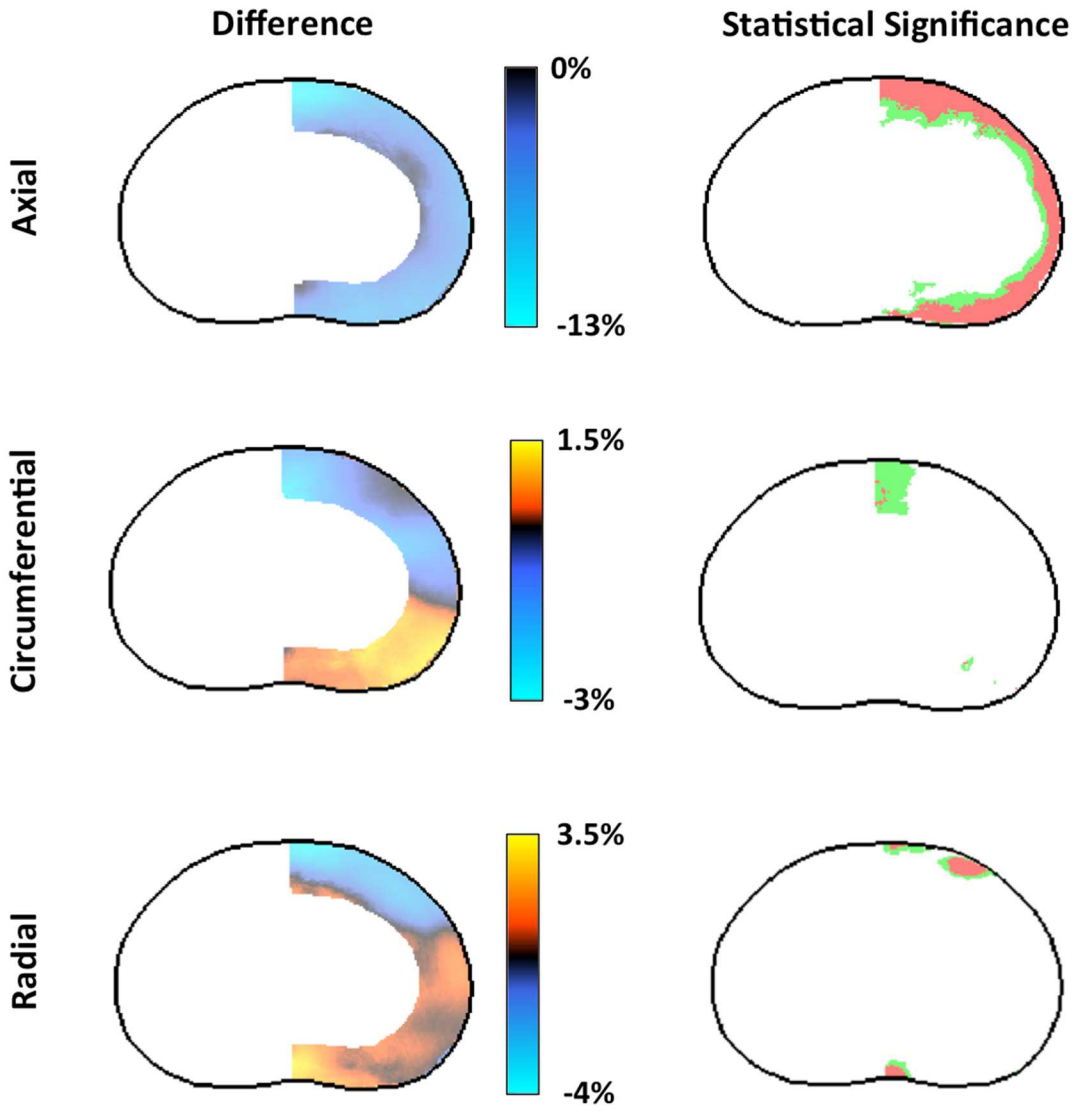

Figure 30: Difference between intact and nucleotomy templates is shown in the first column for all three strain components. Negative values indicate nucleotomy decreased the strain component. Nucleotomy decreased axial strain throughout the annulus. Nucleotomy effects on circumferential and radial strains were less pronounced, although there were regions of decreased strain in the anterior region and increased strain in the posterior. The second column shows the regions where these differences are statistically significant, with red indicating $p < 0.05$ and green $p < 0.1$. All stats have $q < 0.02$, which means that less than 2% of the significant voxels are expected to be false positives.

6.4 Discussion

Strain templates determined the effects of nucleotomy on the internal strains of mildly-degenerate L3-L4 discs. The most notable change caused by nucleotomy was an average 5.6% compressive strain increase throughout the annulus (**Table 4**, **Figure 30A**). This increase in compressive strain for the same applied load was expected due to the loss of internal disc pressure that occurred as a result of nucleotomy.

While the magnitude of compressive strain increased throughout the annulus, circumferential and radial strains decreased in the anterior regions while increasing in the posterior regions (**Figure 30B&C**). The difference between the anterior and posterior regions, rather than a uniform increase or decrease, may be due to uneven removal of the nucleus pulposus in the nucleotomy procedure. Because the annular incision is in the posterior region of the disc, it is easier to remove tissue from the anterior nucleus than the posterior using pituitary rongeours. While NP material has been shown to redistribute and rehydrate following nucleotomy,[60; 124] it is not completely fluid and may remain more damaged in the anterior region than posterior. As a result, when compressed, it would exert less pressure in the anterior region, allowing for less radial and circumferential strains in the anterior region despite the increase in compressive strain. In contrast, with a relatively intact nucleus pulposus in the posterior region, the greater compressive strains were accompanied by increases in circumferential and radial

strains. The increase from 3.3±0.6% circumferential strain to 4.3±0.4% strain in the posterolateral region may be especially relevant, because this is the disc region most prone to annular tears.

There were a number of similarities in the internal strain distributions of the intact L3-L4 template created for this study with the intact L4-L5 template created in chapter 5. For example, the amount of axial strain was lowest in the anterior region and circumferential strain was highest in the lateral region, with a corresponding minimum of radial strain in the lateral region (**Figure 21** and **Figure 28**). There were also a number of differences between the strain templates. For example, the range of strain values was greater in the L3-L4 template than in the L4-L5 template. This may be due to the difference in loading protocols. The L4-L5 template had undergone 4 stages of compression and imaging, although data for this work was only taken from the first and last stages. The L3-L4 discs were only imaged once in the unloaded and final loaded conditions. As a result of the longer testing protocol, the L4-L5 disc tissue may have reached equilibrium whereas the L3-L4 discs may not have, which would result in more uniform strain distributions. Also, although the applied compressive strain for both sample sets was approximately 10%, the resulting applied stress of 0.71±0.2 MPa for the L3-L4 discs was double the stress of 0.35 ± 0.2 MPa for the L4-L5 discs. This difference in applied stress is probably due to the difference in degeneration grades between the sample sets, as the less degenerate L3-L4 discs supported more loads for the given displacements. The difference in degeneration grades is also evident in the

geometry measurements of the anatomical templates. For discs of similar degeneration grades, the L3-L4 discs should have a smaller cross-sectional area and lower disc height than the L4-L5 discs. However, the L4-L5 template had a lower disc height than the L3-L4 template (**Figure 27**), which is consistent with a more degenerate sample set.

The difference in disc level, degeneration states, and loading protocols makes the L3-L4 and L4-L5 template unsuitable for more thorough comparisons. Replicating the experiment described in this chapter with degenerate L3-L4 discs would be extremely useful in studying internal disc strain distributions. A two-dimensional study of disc strain found nucleotomy increased radial and circumferential strains more substantially in degenerate samples than non-degenerate.[104] Therefore, it is likely that the increase in posterolateral circumferential strain found in this work would be even greater in more degenerate samples, indicating a region susceptible to structural damage.

While this study demonstrated the changes in strain magnitude and distribution caused by nucleotomy, it also leaves a number of questions to be answered in future studies. First, the significant changes in strain in the posterolateral region were measured on the uninjured side of the disc. The strains in the region immediately surrounding the nucleotomy incision have not been measured. Such measurements would be useful not only to determine the incision's effects, but also would serve as a first step towards examining the local strains around radial tears. Second, as was noted in section 7.2.1, a number of prepared

samples had imaging artifacts that prevented their inclusion in the data set. These artifacts presented as large voids near the superior edge of the disc and were due to inhomogeneity within the magnetic field while imaging. Reducing the field inhomogeneity by performing these experiments using a 3T scanner may improve the robustness of the sequence and will be discussed in more detail in section 8.2.1.

In conclusion, this study showed that nucleotomy increases axial strain, and increases circumferential strain in the posterior and posterolateral regions. This strain increase may leave the tissue more susceptible to further injury, such as annular tears. The experiment also demonstrates the feasibility of comparing treatments using templates.

CHAPTER 7: CONCLUSIONS AND FUTURE DIRECTIONS

7.1 Summary of Experimental Findings

The objective of this dissertation was to quantify the mechanical contributions of the nucleus pulposus to the function of the intervertebral disc in compressive loading. In the cyclic loading experiment described in chapter 3, removal of the nucleus pulposus caused acute changes to the disc's mechanical response such as a decrease in compressive stiffness with an accompanying increase in compressive strain. These changes correspond to hypermobility, which will alter overall spinal mechanics and may impact low back pain via altered motion throughout the spinal column. In addition to these acute changes, nucleotomy also decreased the fluid-flow related effects of compressive loading. Chapter 4 used the nucleotomy cyclic loading data as a control to evaluate the effectiveness of a hydrogel implant as a nucleus pulposus replacement. The implant did not significantly affect the compressive modulus or strain of the samples, but was not expelled during the extensive testing and preserved the creep response of the discs.

Chapter 5 focused on technical developments to study internal disc mechanics. Specifically, an intervertebral disc strain template of moderately degenerate L4-L5 discs undergoing axial compressive strain was created. The strain template facilitates the study of group-level trends in strain distribution while reducing the effects of individual variations between samples. The template showed that internal strain varied widely, despite the uniform compressive strain. Axial

strains were highest in the vulnerable posterolateral and posterior regions. Circumferential strains were highest in the lateral region, with a corresponding minimum in radial strain in that region. In chapter 6, the strain template was used to validate the internal strains predicted by a recently created finite element model of the intervertebral disc.

The strain template technique was used to evaluate the effects of nucleotomy on the internal strain of mildly-degenerate human L3-L4 discs in chapter 7. Removal of the nucleus increased axial strain throughout the annulus fibrosus, consistent with the existing literature stating that the nucleus plays a significant role in supporting compressive loads. Removal of the nucleus also unevenly altered the distribution of circumferential and radial strains within the annulus. Circumferential strain was significantly higher in the posterolateral region, which may substantially increase the risk of annular tears in that region.

7.2 Future Directions

7.2.1 Technical Developments

The MR imaging sequence that was recently developed coupled with the template analysis method described in chapter 5 are vast improvements on the previous methods of measuring internal strain. However, there is room to make the techniques more robust and widely applicable. In particular, adapting the current imaging sequence for use on a 3T MR scanner would have a number of advantages. First, the 7T whole-body scanner used for this study is much less common than a 3T

scanner. Developing a sequence suitable for the 3T scanner would facilitate more widespread use of the techniques.

A second advantage to using a 3T magnet would be a reduction in magnetic field inhomogeneity artifacts. Inhomogeneity artifacts are more common at high magnetic fields and can lead to image distortion and loss of signal at tissue interfaces.[156] Within this work, these artifacts were manifested by severe signal loss at the bone-disc interface (**Figure 31A**). The magnetic field was manually adjusted, or shimmed, to be made more homogeneous in the immediate vicinity of the disc, thereby reducing or eliminating the artifact (**Figure 31B**). However, the shimming process is an optimization of 9 separate parameters and could not sufficiently eliminate the artifacts in nearly half of the samples tested. Unfortunately, while reducing the strength of the magnetic field from 7T to 3T would reduce inhomogeneity artifacts, it would also reduce image contrast. However, given the quality of other 3T images used for strain measurements,[30; 102] it is reasonable to expect that proper sequence development could produce 3D images using a 3T scanner that are suitable for strain measurements.

The comparison of internal strains between the strain template and the finite element model in chapter 5 also uncovered a couple of methods to improve the finite element model's functionality. First, the model geometry can be adjusted to match the superior and inferior contours of the template geometry. Second, the elements in the posterior region need to be refined to eliminate potential discontinuities in the modeling of the collagen fibers. These adjustments will yield a

more robust and thoroughly validated finite element model that is capable of performing a wide range of disc biomechanics studies.

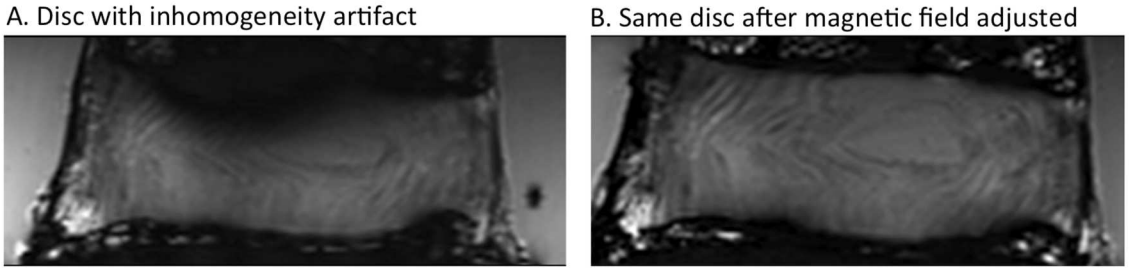

Figure 31: Intervertebral disc with inhomogeneity artifact at superior bone-disc interface (A) and artifact removed following adjustment to the magnetic field (B).

7.2.2 Additional Experimental Studies

The comparison of the intact and nucleotomy samples is but one example of the many studies that can be done to examine the internal strains of the intervertebral disc. A close companion to the current work would be to determine the strains in the region surrounding the nucleotomy incision. Because the AF is disrupted in the incision, the local tissue strain in the incision regions would most likely be higher than the uninjured tissue. Quantifying the amount of change and size of the region in which tissue strains are affected would be valuable in assessing the long-term effects of this common medical procedure. The incision study would also be a first step towards examining the effects of naturally occurring annulus tears. Annular tears are very common, with defects such as tears in the posterior annulus occurring in 70-90% of adults. [143] Despite their prevalence, understanding of how these tears originate or propagate is limited. Understanding how such

defects affect the local tissue strain would be a significant improvement in understanding disc mechanics.

Another study directly related to the current work would be to repeat the nucleotomy experiment with moderately and severely degenerate discs. In the cyclic loading experiments, nucleotomy caused greater changes in the degenerate samples than the intact ones. It would be relevant to determine the commensurate changes in internal strain. These experiments could be extended to examine other physiologically relevant and more strenuous loading conditions, such as lateral bending and torsion.

Because of the positive outcomes of testing the hydrogel implant in chapter 4, studies have been initiated to evaluate the disc in a large animal model. However, the implant's effect on the 3D internal strains has not yet been studied, and would be relevant to evaluating the implant's effectiveness at restoring or maintaining disc mechanical properties. Treatment effectiveness would be especially relevant using moderate and severely degenerate discs, rather than the mildly degenerate discs used in the nucleotomy study. Tissue strain could also be used to evaluate other treatments under development, such as annulus fibrosus repair and tissue engineered discs.[47; 85; 150] Evaluating how closely these treatments match native strain distributions would be an important indicator of treatment effectiveness.

7.3 Final Conclusions

In conclusion, the nucleus pulposus plays an important role in supporting compressive loads within the disc. Removal of the nucleus pulposus caused acute

changes to the disc's mechanical response that correspond to hypermobility. In addition to these acute changes, nucleotomy also decreased the fluid-flow related effects of compressive loading. In mildly-degenerate human discs, removal of the nucleus increased axial strain throughout the annulus fibrosus. The procedure also unevenly altered the distribution of circumferential and radial strains within the annulus. Nucleotomy caused substantially higher circumferential strain in the posterolateral region, which increases the risk of annular tears. The tools developed in this work and the experimental work can be utilized to understand and design treatments for disc degeneration.

BIBLIOGRAPHY

1. Adams MA, Dolan P, Hutton WC. 1987. Diurnal Variations in the Stresses on the Lumbar Spine. Spine 12:130-137.
2. Adams MA, Dolan P, Hutton WC, et al. 1990. Diurnal Changes in Spinal Mechanics and Their Clinical Significance. Journal of Bone and Joint Surgery 72B:266-270.
3. Adams MA, Freeman BJC, Morrison HP, et al. 2000. Mechanical Initiation of Intervertebral Disc Degeneration. Spine 25:1625-1636.
4. Adams MA, Hutton WC. 1985. Gradual Disc Prolapse. Spine 10:524-531.
5. Adams MA, McNally DS, Dolan P. 1996. 'Stress' Distributions inside Intervertebral Discs. The Effects of Age and Degeneration. Journal of Bone and Joint Surgery 78:965-972.
6. Adams MA, Roughley PJ. 2006. What Is Intervertebral Disc Degeneration, and What Causes It? Spine 31:2151-2161.
7. Ahrens M, Tsantrizos A, Donkersloot P, et al. 2009. Nucleus Replacement with the Dascor Disc Arthroplasty Device: Interim Two-Year Efficacy and Safety Results from Two Prospective, Non-Randomized Multicenter European Studies. Spine 34:1376-1384.
8. Allen MJ, Schoonmaker JE, Bauer TW, et al. 2004. Preclinical Evaluation of a Poly (Vinyl Alcohol) Hydrogel Implant as a Replacement for the Nucleus Pulposus. Spine 29:515-523.
9. Andersson GBJ. 1999. Epidemiological Features of Chronic Low-Back Pain. The Lancet 354:581-585.
10. Antoniou J, Steffen T, Nelson F, et al. 1996. The Human Lumbar Intervertbral Disc: Evidence for Changes in the Biosynthesis and Denaturation of the Extracellular Matrix with Growth, Maturation, Ageing, and Degeneration. Journal of Clinical Investigation 98:996-1003.
11. Avants B, Duda JT, Kim J, et al. 2008. Multivariate Analysis of Structural and Diffusion Imaging in Traumatic Brain Injury. Academic radiology 15:1360-1375.
12. Avants BB, Tustison NJ, Song G, et al. 2011. A Reproducible Evaluation of Ants Similarity Metric Performance in Brain Image Registration. Neuroimage 54:2033-2044.
13. Baer AE, Laursen TA, Guilak F, et al. 2003. The Micromechanical Environment of Intervertebral Disc Cells Determined by a Finite Deformation, Anisotropic, and Biphasic Finite Element Model. Journal of Biomechanical Engineering 125:1-11.
14. Balkovec C, Vernengo J, McGill SM. 2013. The Use of a Novel Injectable Hydrogel Nucleus Pulposus Replacement in Restoring the Mechanical Properties of Cyclically Fatigued Porcine Intervertebral Discs. J Biomech Eng 135:61004-61005.

15. Beckstein JC, Sen S, Schaer TP, et al. 2008. Comparison of Animal Discs Used in Disc Research to Human Lumbar Disc: Axial Compression Mechanics and Glycosaminoglycan Content. Spine 33:E166-E173.
16. Bertagnoli R, Kumar S. 2002. Indications for Full Prosthetic Disc Arthroplasty: A Correlation of Clinical Outcome against a Variety of Indications. Eur Spine J 11:S131-S136.
17. Bertagnoli R, Sabatino CT, Edwards JT, et al. 2005. Mechanical Testing of a Novel Hydrogel Nucleus Replacement Implant. Spine J 5:672-681.
18. Bowden AE, Rabbitt RD, Weiss JA. 1998. Anatomical Registration and Segmentation by Warping Template Finite Element Models. pp. 469-476.
19. Boxberger JI, Sen S, Yerramalli CS, et al. 2006. Nucleus Pulposus Glycosaminoglycan Content Is Correlated with Axial Mechanics in Rat Lumbar Motion Segments. Journal of Orthopaedic Research 24:1906-1915.
20. Brickley-Parsons D, Glimcher MJ. 1984. Is the Chemistry of Collagen in Intervertebral Discs an Expression of Wolff's Law? A Study of the Human Lumbar Spine. Spine 9:148-163.
21. Brinckmann P, Grootenboer H. 1991. Change of Disc Height, Radial Disc Bulge, and Intradiscal Pressure from Discectomy. An in Vitro Investigation on Human Lumbar Discs. Spine 16:641-646.
22. Brinckmann P, Johannleweling N, Hilweg D, et al. 1987. Fatigue Fracture of Human Lumbar Vertebrae. Clinical Biomechanics 2:94-96.
23. Bron JL, Helder MN, Meisel HJ, et al. 2009. Repair, Regenerative and Supportive Therapies of the Annulus Fibrosus: Achievements and Challenges. Eur Spine J 18:301-313.
24. Buckwalter JA, Einhorn TA, Simon SR. 2000. Orthopaedic Basic Science: Biology and Biomechanics of the Musculoskeletal System: American Academy of Orthopaedic Surgeons;
25. Cannella M, Arthur A, Allen S, et al. 2008. The Role of the Nucleus Pulposus in Neutral Zone Human Lumbar Intervertebral Disc Mechanics. J Biomech 41:2104-2111.
26. Carragee EJ, Paragioudakis SJ, Khurana S. 2000. Lumbar High-Intensity Zone and Discography in Subjects without Low Back Problems. Spine 25:2987-2992.
27. Castro WHM, Jerosch J, Halm H, et al. 1992. How Much Nuclear Material Is Removed with Percutaneous Nucleotomy. Z Orthop Grenzg 130:467-471.
28. Cercignani M, Embleton K, Parker GJM, et al. 2012. Group-Averaged Anatomical Connectivity Mapping for Improved Human White Matter Pathway Visualisation. NMR in Biomedicine 25:1224-1233.
29. Chan DD, Gossett PC, Butz KD, et al. 2014. Comparison of Intervertebral Disc Displacements Measured under Applied Loading with Mri at 3.0 T and 9.4 T. J Biomech 47:2801-2806.
30. Chan DD, Neu CP. 2013. Intervertebral Disc Internal Deformation Measured by Displacements under Applied Loading with Mri at 3t. Magn Reson Med.

31. Chan SC, Ferguson SJ, Gantenbein-Ritter B. 2011. The Effects of Dynamic Loading on the Intervertebral Disc. European spine journal : official publication of the European Spine Society, the European Spinal Deformity Society, and the European Section of the Cervical Spine Research Society 20:1796-1812.
32. Cloyd J, Malhotra N, Weng L, et al. 2007. Material Properties in Unconfined Compression of Human Nucleus Pulposus, Injectable Hyaluronic Acid-Based Hydrogels and Tissue Engineering Scaffolds. Eur Spine J 16:1892-1898.
33. Coric D, Mummaneni PV. 2008. Nucleus Replacement Technologies. Journal of neurosurgery Spine 8:115-120.
34. Cortes DH, Jacobs NT, Delucca JF, et al. 2014. Elastic, Permeability and Swelling Properties of Human Intervertebral Disc Tissues: A Benchmark for Tissue Engineering. J Biomech 47:2088-2094.
35. Dahl MC, Ellingson AM, Mehta HP, et al. 2013. The Biomechanics of a Multilevel Lumbar Spine Hybrid Using Nucleus Replacement in Conjunction with Fusion. The Spine Journal 13:175-183.
36. Datta R, Lee J, Duda J, et al. 2012. A Digital Atlas of the Dog Brain. PLoS One 7:e52140.
37. Demers CN, Antoniou J, Mwale F. 2004. Value and Limitations of Using the Bovine Tail as a Model for the Human Lumbar Spine. Spine 29:2793-2799.
38. DiAngelo DJ, Foley KT, Morrow BR, et al. 2004. In Vitro Biomechanics of Cervical Disc Arthroplasty with the Prodisc-C Total Disc Implant. Neurosurgical Focus 17:44-54.
39. Dullerud R, Amundsen T, Johansen JG, et al. 1993. Lumbar Percutaneous Automated Nucleotomy - Technique, Patient Selection, and Preliminary Results. Acta Radiologica 34:536-542.
40. Elliott DM, Sarver JJ. 2004. Young Investigator Award Winner: Validation of the Mouse and Rat Disc as Mechanical Models of the Human Lumbar Disc. Spine 29:713-722.
41. Fountas KN, Kapsalaki EZ, Feltes CH, et al. 2004. Correlation of the Amount of Disc Removed in a Lumbar Microdiscectomy with Long-Term Outcome. Spine 29:2521-2524.
42. Frei H, Oxland TR, Rathonyi GC, et al. 2001. The Effect of Nucleotomy on Lumbar Spine Mechanics in Compression and Shear Loading. Spine 26:2080-2089.
43. Friedman WA. 1983. Percutaneous Discectomy - an Alternative to Chemonucleolysis. Neurosurgery 13:542-547.
44. Gibson JNA, Grant IC, Waddell G. 1999. The Cochrane Review of Surgery for Lumbar Disc Prolapse and Degenerative Lumbar Spondylosis. Spine 24:1820-1832.
45. Gilchrist CL, Xia JQ, Setton LA, et al. 2004. High-Resolution Determination of Soft Tissue Deformations Using Mri and First-Order Texture Correlation. IEEE transactions on medical imaging 23:546-553.

46. Goel VK, Nishiyama K, Weinstein JN, et al. 1986. Mechanical Properties of Lumbar Spinal Motion Segments as Affected by Partial Disc Removal. Spine 11:1008-1012.
47. Grunert P, Gebhard HH, Bowles RD, et al. 2014. Tissue-Engineered Intervertebral Discs: Mri Results and Histology in the Rodent Spine. J Neurosurg Spine 20:443-451.
48. Haefeli M, Kalberer F, Saegesser D, et al. 2006. The Course of Macroscopic Degeneration in the Human Lumbar Intervertebral Disc. Spine 31:1522-1531.
49. Han WM, Heo SJ, Driscoll TP, et al. 2013. Macro- to Microscale Strain Transfer in Fibrous Tissues Is Heterogeneous and Tissue-Specific. Biophys J 105:807-817.
50. Han WM, Nerurkar NL, Smith LJ, et al. 2012. Multi-Scale Structural and Tensile Mechanical Response of Annulus Fibrosus to Osmotic Loading. Ann Biomed Eng 40:1610-1621.
51. Harris MD, Anderson AE, Henak CR, et al. 2012. Finite Element Prediction of Cartilage Contact Stresses in Normal Human Hips. Journal of Orthopaedic Research 30:1133-1139.
52. Hasegawa K, Turner C, Chen J, et al. 1995. Effect of Disc Lesion on Microdamage Accumulation in Lumbar Vertebrae under Cyclic Compression Loading. Clinical Orthopaedics & Related Research:190-198.
53. Heneghan P, Riches PE. 2008. The Strain-Dependent Osmotic Pressure and Stiffness of the Bovine Nucleus Pulposus Apportioned into Ionic and Non-Ionic Contributors. J Biomech 41:2411-2416.
54. Heuer F, Ulrich S, Claes LE, et al. 2008. Biomechanical Evaluation of Conventional Anulus Fibrosus Closure Methods Required for Nucleus Replacement. Journal of Neurosurgery: Spine 9:307-313.
55. Hickey DS, Hukins DWL. 1980. Relation between the Structure of the Annulus Fibrosus and the Function and Failure of the Intervertebral Disc. Spine 5:106-116.
56. Hilibrand AS, Robbins M. 2004. Adjacent Segment Degeneration and Adjacent Segment Disease: The Consequences of Spinal Fusion? The Spine Journal 4:S190-S194.
57. Iatridis JC, ap Gwynn I. 2004. Mechanisms for Mechanical Damage in the Intervertebral Disc Annulus Fibrosus. J Biomech 37:1165-1175.
58. Iatridis JC, Setton LA, Foster RJ, et al. 1998. Degeneration Affects the Anisotropic and Nonlinear Behaviors of Human Anulus Fibrosus in Compression. J Biomech 31:535-544.
59. Iatridis JC, Setton LA, Weidenbaum M, et al. 1997. Alterations in the Mechanical Behavior of the Human Lumbar Nucleus Pulposus with Degeneration and Aging. Journal of Orthopaedic Research 15:318-322.
60. Iatridis JC, Weidenbaum M, Setton LA, et al. 1996. Is the Nucleus Pulposus a Solid or a Fluid? Mechanical Behaviors of the Nucleus Pulposus of the Human Intervertebral Disc. Spine 21:1174-1184.

61. Ishihara H, Tsuji H, Hirano N, et al. 1993. Biorheological Responses of the Intact and Nucleotomized Intervertebral Disks to Compressive, Tensile, and Vibratory Stresses. Clinical Biomechanics 8:250-254.
62. Jacobs NT, Cortes DH, Peloquin JM, et al. 2014. Validation and Application of an Intervertebral Disc Finite Element Model Utilizing Independently Constructed Tissue-Level Constitutive Formulations That Are Nonlinear, Anisotropic, and Time-Dependent. J Biomech 47:2540-2546.
63. Johannessen W, Cloyd J, O'Connell G, et al. 2006. Trans-Endplate Nucleotomy Increases Deformation and Creep Response in Axial Loading. Annals of Biom Eng 34:687-696.
64. Johannessen W, Vresilovic EJ, Wright AC, et al. 2004. Intervertebral Disc Mechanics Are Restored Following Cyclic Loading and Unloaded Recovery. Annals of Biom Eng 32:70-76.
65. Joshi A, Massey CJ, Karduna A, et al. 2009. The Effect of Nucleus Implant Parameters on the Compressive Mechanics of the Lumbar Intervertebral Disc: A Finite Element Study. Journal of Biomedical Materials Research Part B-Applied Biomaterials 90B:596-607.
66. Kambin P, Brager MD. 1987. Percutaneous Posterolateral Discectomy - Anatomy and Mechanism. Clinical Orthopaedics and Related Research:145-154.
67. Katz JN. 2006. Lumbar Disc Disorders and Low-Back Pain: Socioeconomic Factors and Consequences. Journal of Bone and Joint Surgery 88A:21-24.
68. Kerttula L, Kurunlahti M, Jauhiainen J, et al. 2001. Apparent Diffusion Coefficients and T2 Relaxation Time Measurements to Evaluate Disc Degeneration. A Quantitative Mr Study of Young Patients with Previous Vertebral Fracture. Acta radiologica (Stockholm, Sweden : 1987) 42:585-591.
69. Kikinis R, Shenton ME, Iosifescu DV, et al. 1996. A Digital Brain Atlas for Surgical Planning, Model-Driven Segmentation, and Teaching. Ieee Transactions on Visualization and Computer Graphics 2:232-241.
70. Koeller W, Funke F, Hartmann F. 1984. Biomechanical Behavior of Human Intervertebral Discs Subjected to Long Lasting Axial Loading. Biorheology 21:675-686.
71. Korecki CL, MacLean JJ, Iatridis JC. 2008. Dynamic Compression Effects on Intervertebral Disc Mechanics and Biology. Spine 33:1403-1409.
72. Kumar D, Gerges I, Tamplenizza M, et al. 2014. Three-Dimensional Hypoxic Culture of Human Mesenchymal Stem Cells Encapsulated in a Photocurable, Biodegradable Polymer Hydrogel: A Potential Injectable Cellular Product for Nucleus Pulposus Regeneration. Acta Biomater 10:3463-3474.
73. Kurtz SM, van Ooij A, Ross R, et al. 2007. Polyethylene Wear and Rim Fracture in Total Disc Arthroplasty. The Spine Journal 7:12-21.
74. Laible JP, Pflaster DS, Krag MH, et al. 1993. A Poroelastic-Swelling Finite-Element Model with Application to the Intervertebral Disc. Spine 18:659-670.
75. Lalys F, Haegelen C, Ferre J-C, et al. 2010. Construction and Assessment of a 3-T Mri Brain Template. NeuroImage 49:345-354.

76. Lewis G. 2012. Nucleus Pulposus Replacement and Regeneration/Repair Technologies: Present Status and Future Prospects. J Biom Mat Res 100B:1702-1720.
77. Li Y, Lewis G. 2010. Influence of Surgical Treatment for Disc Degeneration Disease at C5-C6 on Changes in Some Biomechanical Parameters of the Cervical Spine. Medical Engineering & Physics 32:595-603.
78. Liebscher T, Haefeli M, Wuertz K, et al. 2011. Age-Related Variation in Cell Density of Human Lumbar Intervertebral Disc. Spine 36:153-159.
79. Luo X, Pietrobon R, X Sun S, et al. 2004. Estimates and Patterns of Direct Health Care Expenditures among Individuals with Back Pain in the United States. Spine 29:79-86.
80. Malhotra NR, Han WM, Beckstein J, et al. 2012. An Injectable Nucleus Pulposus Implant Restores Compressive Range of Motion in the Ovine Disc. Spine 37:E1099-E1105.
81. Marchand F, Ahmed AM. 1990. Investigation of the Laminate Structure of the Lumbar Disc Anulus Fibrosus. Spine 15:402-410.
82. Marinelli NL, Haughton VM, Anderson PA. 2010. T2 Relaxation Times Correlated with Stage of Lumbar Intervertebral Disk Degeneration and Patient Age. American Journal of Neuroradiology 31:1278-1282.
83. Markolf KL, Morris JM. 1974. The Structural Components of the Intervertebral Disc: A Study of Their Contributions to the Ability of the Disc to Withstand Compressive Forces. Journal of bone and Joint Surgery 56A:675-687.
84. Marquardt G, Bruder M, Theuss S, et al. 2012. Ultra-Long-Term Outcome of Surgically Treated Far-Lateral, Extraforaminal Lumbar Disc Herniations: A Single-Center Series. Eur Spine J 21:660-665.
85. Martin JT, Milby AH, Chiaro JA, et al. 2014. Translation of an Engineered Nanofibrous Disc-Like Angle-Ply Structure for Intervertebral Disc Replacement in a Small Animal Model. Acta Biom 10:2473-2481.
86. Massey CJ, van Donkelaar CC, Vresilovic E, et al. 2012. Effects of Aging and Degeneration on the Human Intervertebral Disc During the Diurnal Cycle: A Finite Element Study. Journal of Orthopaedic Research 30:122-128.
87. McKinley M, O'Loughlin VD. 2006. Human Anatomy. Boston: McGraw Hill;
88. Meakin JR, Hukins DWL. 2000. Effect of Removing the Nucleus Pulposus on the Deformation of the Annulus Fibrosus During Compression of the Intervertebral Disc. J Biomech 33:575-580.
89. Meakin JR, Redpath TW, Hukins DWL. 2001. The Effect of Partial Removal of the Nucleus Pulposus from the Intervertebral Disc on the Response of the Human Annulus Fibrosus to Compression. Clinical Biomechanics 16:121-128.
90. Michalek AJ, Iatridis JC. 2011. Penetrating Annulus Fibrosus Injuries Affect Dynamic Compressive Behaviors of the Intervertebral Disc Via Altered Fluid Flow: An Analytical Interpretation. Journal of Biomechanical Engineering 133:084502.

91. Mirza SK, Deyo RA. 2007. Systematic Review of Randomized Trials Comparing Lumbar Fusion Surgery to Nonoperative Care for Treatment of Chronic Back Pain. Spine 32:816-823.
92. Mochida J, Nishimura K, Nomura T, et al. 1996. The Importance of Preserving Disc Structure in Surgical Approaches to Lumbar Disc Herniation. Spine 21:1556-1563; discussion 1563-1554.
93. Moore RJ. 2000. The Vertebral End-Plate: What Do We Know? Eur Spine J 9:92-96.
94. Mulholland RC. 2012. The Michel Benoist and Robert Mulholland Yearly European Spine Journal Review: A Survey of the "Surgical and Research" Articles in the European Spine Journal, 2011. European spine journal: official publication of the European Spine Society, the European Spinal Deformity Society, and the European Section of the Cervical Spine Research Society 21:195-203.
95. Murphy K, van Ginneken B, Reinhardt JM, et al. 2011. Evaluation of Registration Methods on Thoracic Ct: The Empire10 Challenge. IEEE transactions on medical imaging 30:1901-1920.
96. Nachemson AL. 1981. Disc Pressure Measurements. Spine 6:93-97.
97. Natarajan RN, Andersson GBJ, Patwardhan AG, et al. 2002. Effect of Annular Incision Type on the Change in Biomechanical Properties in a Herniated Lumbar Intervertebral Disc. Journal of Biomechanical Engineering-Transactions of the Asme 124:229-236.
98. Natarajan RN, Williams JR, Andersson GBJ. 2004. Recent Advances in Analytical Modeling of Lumbar Disc Degeneration. Spine 29:2733-2741.
99. Natarajan RN, Williams JR, Andersson GBJ. 2006. Modeling Changes in Intervertebral Disc Mechanics with Degeneration. J Bone Joint Surg-Am Vol 88A:36-40.
100. Niemeyer F, Wilke H-J, Schmidt H. 2012. Geometry Strongly Influences the Response of Numerical Models of the Lumbar Spine-a Probabilistic Finite Element Analysis. J Biomech 45.
101. O'Connell GD, Jacobs NT, Sen S, et al. 2011. Axial Creep Loading and Unloaded Recovery of the Human Intervertebral Disc and the Effect of Degeneration. Journal of the Mechanical Behavior of Biomedical Materials 4:933-942.
102. O'Connell GD, Johannessen W, Vresilovic EJ, et al. 2007. Human Internal Disc Strains in Axial Compression Measured Noninvasively Using Magnetic Resonance Imaging. Spine 32:2860-2868.
103. O'Connell GD, Vresilovic EJ, Elliott DM. 2007. Comparison of Animals Used in Disc Research to Human Lumbar Disc Geometry. Spine 32:328-333.
104. O'Connell G, Malhotra NR, Vresilovic EJ, et al. 2011. The Effect of Nucleotomy and the Dependence on Degeneration of Human Intervertebral Disc Strain in Axial Compression. Spine 36:1765-1771.
105. Omlor G, Nerlich A, Lorenz H, et al. 2012. Injection of a Polymerized Hyaluronic Acid/Collagen Hydrogel Matrix in an in Vivo Porcine Disc Degeneration Model. Eur Spine J 21:1700-1708.

106. Omlor GW, Fischer J, Kleinschmitt K, et al. 2014. Short-Term Follow-up of Disc Cell Therapy in a Porcine Nucleotomy Model with an Albumin-Hyaluronan Hydrogel: In Vivo and in Vitro Results of Metabolic Disc Cell Activity and Implant Distribution. European spine journal : official publication of the European Spine Society, the European Spinal Deformity Society, and the European Section of the Cervical Spine Research Society.
107. Pelletier MH, Cohen CS, Ducheyne P, et al. 2013. Restoring Segmental Biomechanics through Nucleus Augmentation: An in Vitro Study. J Spinal Disord Tech.
108. Peloquin JM, Yoder JH, Jacobs NT, et al. 2014. Human L3l4 Intervertebral Disc Mean 3d Shape, Modes of Variation, and Their Relationship to Degeneration. J Biomech 47:2452-2459.
109. Peroglio M, Grad S, Mortisen D, et al. 2011. Injectable Thermoreversible Hyaluronan-Based Hydrogels for Nucleus Pulposus Cell Encapsulation. Eur Spine J:1-11.
110. Pfirrmann CWA, Metzdorf A, Zanetti M, et al. 2001. Magnetic Resonance Classification of Lumbar Intervertebral Disc Degeneration. Spine 26:1873-1878.
111. Qasim M, Natarajan RN, An HS, et al. 2012. Initiation and Progression of Mechanical Damage in the Intervertebral Disc under Cyclic Loading Using Continuum Damage Mechanics Methodology: A Finite Element Study. J Biomech 45:1934-1940.
112. Raj PP. 2008. Intervertebral Disc: Anatomy-Physiology-Pathophysiology-Treatment. Pain practice : the official journal of World Institute of Pain 8:18-44.
113. Rajaee SS, Bae HW, Kanim LEA, et al. 2012. Spinal Fusion in the United States. Spine 37:67-76.
114. Reitmaier S, Shirazi-Adl A, Bashkuev M, et al. 2012. In Vitro and in Silico Investigations of Disc Nucleus Replacement. Journal of the Royal Society Interface 9:1869-1879.
115. Reitmaier S, Wolfram U, Ignatius A, et al. 2012. Hydrogels for Nucleus Replacement—Facing the Biomechanical Challenge. Journal of the Mechanical Behavior of Biomedical Materials 14:67-77.
116. Rhee JM, Schaufele M, Abdu WA. 2006. Radiculopathy and the Herniated Lumbar Disccontroversies Regarding Pathophysiology and Management. The Journal of Bone & Joint Surgery 88:2070-2080.
117. Rodrigues-Pinto R, Richardson SM, Hoyland JA. 2014. An Understanding of Intervertebral Disc Development, Maturation and Cell Phenotype Provides Clues to Direct Cell-Based Tissue Regeneration Therapies for Disc Degeneration. European spine journal : official publication of the European Spine Society, the European Spinal Deformity Society, and the European Section of the Cervical Spine Research Society.

118. Ruan DK, Xin H, Zhang C, et al. 2010. Experimental Intervertebral Disc Regeneration with Tissue-Engineered Composite in a Canine Model. Tissue Engineering: Part A 16:2381-2389.
119. Schroeder Y, Wilson W, Huyghe JM, et al. 2006. Osmoviscoelastic Finite Element Model of the Intervertebral Disc. Eur Spine J 15:S361-371.
120. Seroussi RE, Krag MH, Muller DL, et al. 1989. Internal Deformations of Intact and Denucleated Human Lumbar Discs Subjected to Compression, Flexion, and Extension Loads. Journal of Orthopaedic Research: Official Publication of the Orthopaedic Research Society 7:122-131.
121. Setton LAP, Chen JP. 2004. Cell Mechanics and Mechanobiology in the Intervertebral Disc. Spine 29:2710-2723.
122. Sherman J, Cauthen J, Schoenberg D, et al. 2010. Economic Impact of Improving Outcomes of Lumbar Discectomy. The spine journal : official journal of the North American Spine Society 10.
123. Showalter BL, Beckstein JC, Martin JT, et al. 2012. Comparison of Animal Discs Used in Disc Research to Human Lumbar Disc: Torsion Mechanics and Collagen Content. Spine 37:E900-E907.
124. Showalter BL, Chen W, Elliott DM, et al. Evaluation of an Injectable Hydrogel Treatment to Preserve Human Disc Mechanical Function Undergoing Physiologic Cyclic Loading Followed by Hydrated Recovery. Journal of Biomechanical Engineering In Review.
125. Showalter BL, Malhotra NR, Vresilovic EJ, et al. 2014. Nucleotomy Reduces the Effects of Cyclic Compressive Loading with Unloaded Recovery on Human Intervertebral Discs. J Biomech 47:2633-2640.
126. Sivan S, Merkher Y, Wachtel E, et al. 2006. Correlation of Swelling Pressure and Intrafibrillar Water in Young and Aged Human Intervertebral Discs. Journal of Orthopaedic Research 24:1292-1298.
127. Sivan SS, Roberts S, Urban JP, et al. 2014. Injectable Hydrogels with High Fixed Charge Density and Swelling Pressure for Nucleus Pulposus Repair: Biomimetic Glycosaminoglycan Analogues. Acta Biomater 10:1124-1133.
128. Smith LJ, Gorth DJ, Showalter BL, et al. 2014. In Vitro Characterization of a Stem Cell-Seeded Triple Interpenetrating Network Hydrogel for Functional Regeneration of the Nucleus Pulposus. Tissue Engineering: Part A 20:1841-1849.
129. Stokes IA, Greenapple DM. 1985. Measurement of Surface Deformation of Soft Tissue. J Biomech 18:1-7.
130. Stokes IA, Laible JP, Gardner-Morse MG, et al. 2011. Refinement of Elastic, Poroelastic, and Osmotic Tissue Properties of Intervertebral Disks to Analyze Behavior in Compression. Annals of biomedical engineering 39:122-131.
131. Stokes IAF, Iatridis JC. 2005. Biomechanics of the Spine. In: Mow VC, Huiskes R editors. Basic Orthopaedic Biomechanics and Mechano-Biology. Philadelphia: Lippincott Wiliams & Wilkins; pp. 529-562.

132. Strange DGT, Fisher ST, Boughton PC, et al. 2010. Restoration of Compressive Loading Properties of Lumbar Discs with a Nucleus Implant—a Finite Element Analysis Study. The Spine Journal 10:602-609.
133. Szczesny SE, Elliott DM. 2014. Incorporating Plasticity of the Interfibrillar Matrix in Shear Lag Models Is Necessary to Replicate the Multiscale Mechanics of Tendon Fascicles. J Mech Behav Biomed Mater 40:325-338.
134. Thompson JP, Pearce RH, Schechter MT, et al. 1990. Preliminary Evaluation of a Scheme for Grading the Gross Morphology of the Human Intervertebral Disc. Spine 15:411-415.
135. Thoreson O, Baranto A, Ekström L, et al. 2010. The Immediate Effect of Repeated Loading on the Compressive Strength of Young Porcine Lumbar Spine. Knee Surgery, Sports Traumatology, Arthroscopy 18:694-701.
136. Tustison NJ, Avants BB. 2013. Explicit B-Spline Regularization in Diffeomorphic Image Registration. Frontiers in neuroinformatics 7:39.
137. Upton ML, Gilchrist CL, Guilak F, et al. 2008. Transfer of Macroscale Tissue Strain to Microscale Cell Regions in the Deformed Meniscus. Biophysical Journal 95:2116-2124.
138. Urban JPG, McMullin JF. 1988. Swelling Pressure of the Lumbar Intervertebral Disks - Influence of Age, Spinal Level, Composition, and Degeneration. Spine 13:179-187.
139. Urban JPG, Roberts S. 2003. Degeneration of the Intervertebral Disc. Arthritis Research & Therapy 5:120-130.
140. Urban JPG, Smith S, Fairbank JCT. 2004. Nutrition of the Intervertebral Disc. Spine 29:2700-2709.
141. Van Essen DC. 2002. Windows on the Brain: The Emerging Role of Atlases and Databases in Neuroscience. Current Opinion in Neurobiology 12:574-579.
142. Vernon-Roberts B, Fazzalari NL, Manthey BA. 1997. Pathogenesis of Tears of the Anulus Investigated by Multiple-Level Transaxial Analysis of the T12-L1 Disc. Spine 22:2641-2646.
143. Vernon-Roberts B, Moore RJ, Fraser RD. 2007. The Natural History of Age-Related Disc Degeneration: The Pathology and Sequelae of Tears. Spine 32:2797-2804.
144. Videman T, Nurminen M. 2004. The Occurrence of Anular Tears and Their Relation to Lifetime Back Pain History: A Cadaveric Study Using Barium Sulfate Discography. Spine 29:2668-2676.
145. Vo N, Niedernhofer LJ, Nasto LA, et al. 2013. An Overview of Underlying Causes and Animal Models for the Study of Age-Related Degenerative Disorders of the Spine and Synovial Joints. Journal of orthopaedic research : official publication of the Orthopaedic Research Society 31:831-837.
146. Vresilovic EJ, Johannessen W, Elliott DM. 2006. Disc Mechanics with Trans-Endplate Partial Nucleotomy Are Not Fully Restored Following Cyclic Compressive Loading and Unloaded Recovery. Journal of Biomechanical Engineering 128:823-829.

147. Weinstein JN, Lurie JD, Tosteson TD, et al. 2006. Surgical Vs Nonoperative Treatment for Lumbar Disk Herniation. JAMA: The Journal of the American Medical Association 296:2451-2459.
148. White AA, Panjabi MM. 1990. Clinical Biomechanics of the Spine. Philadelphia: J.B. Lippincott Company;
149. White TL, Malone TR. 1990. Effects of Running on Intervertebral Disc Height. Journal of Orthopaedic and Sports Physical Therapy 12:139-146.
150. Wilke H-JP, Ressel LMD, Heuer FP, et al. 2013. Can Prevention of a Reherniation Be Investigated? Establishment of a Herniation Model and Experiments with an Anular Closure Device. Spine 38:E587-E593.
151. Wilke HJ, Kavanagh S, Neller S, et al. 2001. Effect of a Prosthetic Disc Nucleus on the Mobility and Disc Height of the L4-5 Intervertebral Disc Postnucleotomy. J of Neurosurgery 95:208-214.
152. Wilke HJ, Kettler A, Claes LE. 1997. Are Sheep Spines a Valid Biomechanical Model for Human Spines? Spine 22:2365-2374.
153. Wilke HJ, Neef P, Caimi M, et al. 1999. New in Vivo Measurements of Pressures in the Intervertebral Disc in Daily Life. Spine 24:755-762.
154. Woiciechowsky C, Abbushi A, Zenclussen ML, et al. 2012. Regeneration of Nucleus Pulposus Tissue in an Ovine Intervertebral Disc Degeneration Model by Cell-Free Resorbable Polymer Scaffolds. J Tissue Eng Regen Med:DOI: 10.1002/term.1582.
155. Xu MH, Nowinski WL. 2001. Talairach-Tournoux Brain Atlas Registration Using a Metalforming Principle-Based Finite Element Method. Medical Image Analysis 5:271-279.
156. Yang QX, Wang J, Smith MB, et al. 2004. Reduction of Magnetic Field Inhomogeneity Artifacts in Echo Planar Imaging with Sense and Gesepi at High Field. Magn Reson Med 52:1418-1423.
157. Yoder JH, Peloquin JM, Song G, et al. 2014. Internal Three-Dimensional Strains in Human Intervertebral Discs under Axial Compression Quantified Noninvasively by Magnetic Resonance Imaging and Image Registration. J Biomech Eng 136.
158. Yushkevich PA, Avants BB, Pluta J, et al. 2009. A High-Resolution Computational Atlas of the Human Hippocampus from Postmortem Magnetic Resonance Imaging at 9.4 T. Neuroimage 44:385-398.
159. Yushkevich PA, Piven J, Hazlett HC, et al. 2006. User-Guided 3d Active Contour Segmentation of Anatomical Structures: Significantly Improved Efficiency and Reliability. Neuroimage 31:1116-1128.
160. Zhang H, Qadeer A, Mynarcik D, et al. 2011. Delivery of Rosiglitazone from an Injectable Triple Interpenetrating Network Hydrogel Composed of Naturally Derived Materials. Biomaterials 32:890-898.
161. Zhang Y, Lenart BA, Lee JK, et al. 2014. Histological Features of Endplates of the Mammalian Spine: From Mice to Men. Spine (Phila Pa 1976) 39:E312-317.